

1 **Linking the Mediterranean MIS 5 tephra markers to the Campi Flegrei 109-92 ka**
2 **explosive activity (southern Italy) and refining the chronology of the MIS 5c-d**
3 **millennial-scale climate variability**

4
5 Monaco, L.¹⁻², Palladino, D.M.¹, Albert, P.G.³, Arienzo, I.⁴, Conticelli, S.²⁻⁵, Di Vito, M.⁴, Fabbriozio, A.⁶,
6 D'Antonio, M.⁷, Isaia, R.⁴⁻², Manning, C.J.⁸, Nomade, S.⁹, Pereira, A.¹⁰, Petrosino, P.⁷, Sottili, G.¹,
7 Sulpizio, R.¹¹⁻²⁻¹², Zanchetta, G.¹³⁻², Giaccio, B.^{2-14, *}

8
9 *1 Dipartimento di Scienze della Terra, "Sapienza" Università di Roma, Rome, Italy*

10 *2 Istituto di Geologia Ambientale e Geoingegneria, IGAG-CNR, Rome, Italy*

11 *3 Department of Geography, Swansea University, Swansea, UK*

12 *4 Istituto Nazionale di Geofisica e Vulcanologia, INGV-Osservatorio Vesuviano, Naples, Italy*

13 *5 Dipartimento di Scienze della Terra, Università degli Studi di Firenze, Florence, Italy*

14 *6 Institute of Petrology and Structural Geology, Faculty of Science, Charles University, Albertov 6, 12843 Prague, Czech Republic*

15 *7 Dipartimento di Scienze della Terra, delle Risorse e dell'Ambiente, Università degli Studi di Napoli Federico II, Naples, Italy*

16 *8 Department of Earth Sciences, Royal Holloway, University of London, Egham, UK*

17 *9 Laboratoire de Sciences du Climat et de l'Environnement, UMR 8212, CEA-UVSQ, IPSL and Université de Paris-Saclay, Gif-sur-*
18 *Yvette, France*

19 *10 Université Paris-Saclay, CNRS, UMR 8148 GEOPS, Orsay, 91405, France*

20 *11 Dipartimento di Scienze della Terra e Geoambientali, Aldo Moro-University of Bari, Bari, Italy*

21 *12 Istituto Nazionale di Geofisica e Vulcanologia, Sezione di Bologna, Bologna, Italy*

22 *13 Dipartimento di Scienze della Terra, Università di Pisa, Pisa, Italy*

23 *14 Istituto Nazionale di Geofisica e Vulcanologia, Sezione di Roma, Roma, Italy*

24
25 ** Corresponding author: biagio.giaccio@cnr.it*
26
27

28
29 **ABSTRACT**

30 Explosive activity preceding the ~40 ka Campanian Ignimbrite (CI) eruption in the Neapolitan volcanic area,
31 Southern Italy, has long been speculated based on the occurrences of widespread tephra layers, with a
32 Campanian geochemical signature, such as the C-22, X-5, and X-6, preserved in Mediterranean Marine
33 Isotope Stage (MIS) 5 sedimentary records. However, previous studies of pre-CI pyroclastic units occurring in
34 close proximity of the Neapolitan volcanoes, including Campi Flegrei, Somma-Vesuvius, Ischia and Procida
35 islands, did not allow a conclusive identification of the near-source equivalents of these tephra markers. Here
36 we present a comprehensive characterisation of four pyroclastic units from the Campanian Plain, comprising
37 major and trace element glass compositions, Sr-Nd isotopes and ⁴⁰Ar/³⁹Ar dating. Our data allowed the
38 identification of the medial equivalents of the MIS 5 tephra markers, including the widespread C-22, X-5, and
39 X-6 tephra, and their assignment to previously undocumented Campi Flegrei activity between 109-92 ka. In
40 addition to substantially extending Campi Flegrei explosive activity deeper in time, and thus providing the basis
41 for a reevaluation of its history, our findings provide new precise radioisotopic dating to better constrain the
42 chronology of the millennial scale climatic oscillations of the MIS 5c-d in the Mediterranean area and possibly
43 on a larger scale.

44 1. Introduction

45 Near-vent volcanic successions provide fundamental information for reconstructing the eruption history
46 and dynamics of volcanoes. Proximal exposures, however, often provide only fragmentary records of the past
47 activity of a volcanic system, since deposits of older explosive events can be eroded, not preserved or, more
48 commonly, covered by products of younger eruptions. In contrast, tephra layers preserved in sedimentary
49 successions located far away from the volcanic source and characterised by a continuous sediment
50 accumulation history, can provide detailed and undisturbed records of explosive eruptions for a given volcano,
51 including events that are poorly represented or missing in near-vent sections (e.g., [Paterne et al., 1988](#);
52 [Monaco et al., 2021](#)).

53 This also applies to the Neapolitan volcanic area (Campania, southern Italy), including Campi Flegrei, Ischia,
54 Procida and Somma-Vesuvius ([Fig. 1b](#)), where the intense Late Pleistocene explosive activity (e.g., [Peccerillo,](#)
55 [2017 and reference therein](#)) made the earliest pyroclastic products barely accessible in proximal settings.
56 However, these activities are instead documented in distal sedimentary archives. Indeed, since the first distal
57 marine discoveries of [Keller et al. \(1978\)](#), several occurrences of widespread tephra layers with a Campanian
58 geochemical signature embedded within Marine Isotope Stage 5 (MIS 5) sedimentary successions suggested
59 the occurrence of a major explosive activity that, however, had never been documented in proximal sections
60 of the Neapolitan volcanoes. Among them, the C-22 ([Paterne et al., 1986](#)), X-5 and X-6 ([Keller et al., 1978](#))
61 tephra layers have been traced widely across the central Mediterranean area in several terrestrial (e.g., [Wulf](#)
62 [et al., 2004, 2012, 2018](#); [Marciano et al., 2008](#); [Sulpizio et al., 2010](#); [Giaccio et al., 2012, 2017a](#); [Lucchi et al.,](#)
63 [2013](#); [Regattieri et al., 2015](#); [Donato et al., 2016](#); [Leicher et al., 2016](#); [Zanchetta et al., 2018](#); [Petrosino et al.,](#)
64 [2019](#)) and marine (e.g., [Paterne et al., 1986, 1988, 2008](#); [Bourne et al., 2010, 2015](#); [Insinga et al., 2014](#); [Iorio](#)
65 [et al., 2014](#); [Petrosino et al., 2016](#)) sedimentary archives. Moreover, at least two additional tephras, occurring
66 between the C-22 and X-5 markers, with a similar Neapolitan geochemical signature, are also found in
67 Mediterranean MIS 5 records ([Giaccio et al., 2012, 2017a](#); [Wulf et al., 2012](#); [Leicher et al., 2016](#); [Petrosino et](#)
68 [al., 2016](#); [Table 1](#)).

69 Over the last decades, these widespread tephra layers have been used as remarkable marker horizons for
70 dating, synchronizing, and correlating MIS 5 Mediterranean sedimentary successions, the chronologies of
71 which would have otherwise been poorly determined. With this regard, tephra markers from Neapolitan
72 volcanoes arise as pivotal stratigraphic and chronological tools for paleoclimatic and archaeological
73 investigations at the regional scale (e.g., [Wulf et al., 2012, 2018](#); [Bourne et al., 2015](#); [Regattieri et al., 2015](#);
74 [Leicher et al., 2016](#); [Petrosino et al., 2016](#); [Giaccio et al., 2017a](#); [Zanchetta et al., 2018](#)).

75 Despite their great chronological importance, the lack of near-vent counterparts has left the specific volcanic
76 source of these marker layers still undetermined, leading authors to ascribe them either to an unspecified
77 Campanian volcanism (e.g., [Wulf et al., 2012](#)), or to an undefined Neapolitan volcanic area (e.g., [Giaccio et
78 al., 2017a](#)) or to the so-called “Campanian Volcanic Zone” (CVZ; [Rolandi et al., 2003](#)) (e.g., [Munno and
79 Petrosino, 2007](#)). Furthermore, in terms of tephrochronological applications, precise and accurate radioisotopic
80 ages are currently available only for two of these markers (i.e., X-5 and X-6), and their full geochemical
81 characterization (i.e., major, trace elements, and Sr-Nd composition) in near-vent outcrops is still pending.
82 Such remaining uncertainties on their origins and incompleteness of their geochronological and geochemical
83 characterization, prevent their use for any volcanological purposes and limit their tephrochronological potential.
84 In order to fill the knowledge gap about these tephra markers and exploit their full potential for both
85 volcanological and tephrochronological perspectives, we acquired stratigraphic, geochemical, and
86 geochronological data for five medial-distal (30-60 km from the vent) pyroclastic units, preceding the
87 Campanian Ignimbrite (CI) eruption, outcropping around the eastern rim of the Campanian Plain ([Fig. 1b](#)).
88 Four of these units (Maddaloni, Montemaoro, Canello and Santa Lucia; [Fig. 1b](#)) were previously described
89 ([Di Vito et al., 2008](#)), while a fifth one (i.e., Triflisco) is recognised as a distinct, younger event in this study
90 ([Fig. 1b](#)). The new chemical, isotopic and geochronological data acquired in this study allowed confidently to
91 correlate the five medial-distal fall units to the widespread X-6, X-5, TM-24b/POP-2a, TM-24a/POP2 and C-22
92 marker tephra ([Table 1](#)), attributing them to the 109-92 ka Campi Flegrei explosive activity. Our findings thus
93 extend back in time the explosive history of the Campi Flegrei volcanic field and provide new precise dating
94 for refining the chronology of the millennial-scale climatic oscillations of the MIS 5c-d in the Mediterranean
95 area.

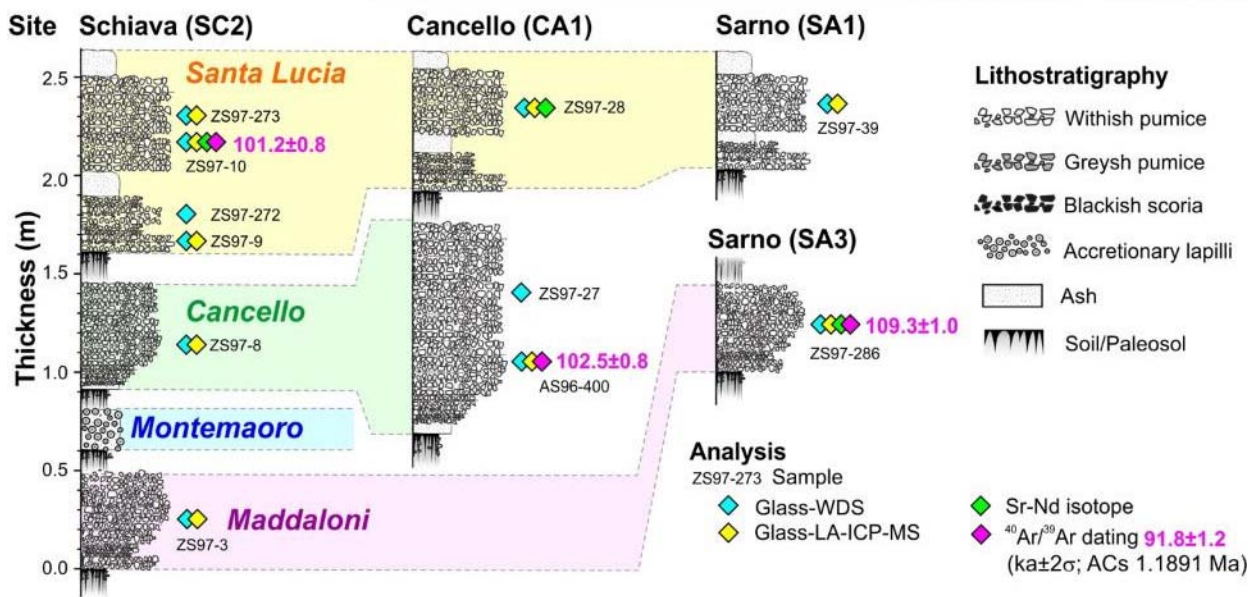
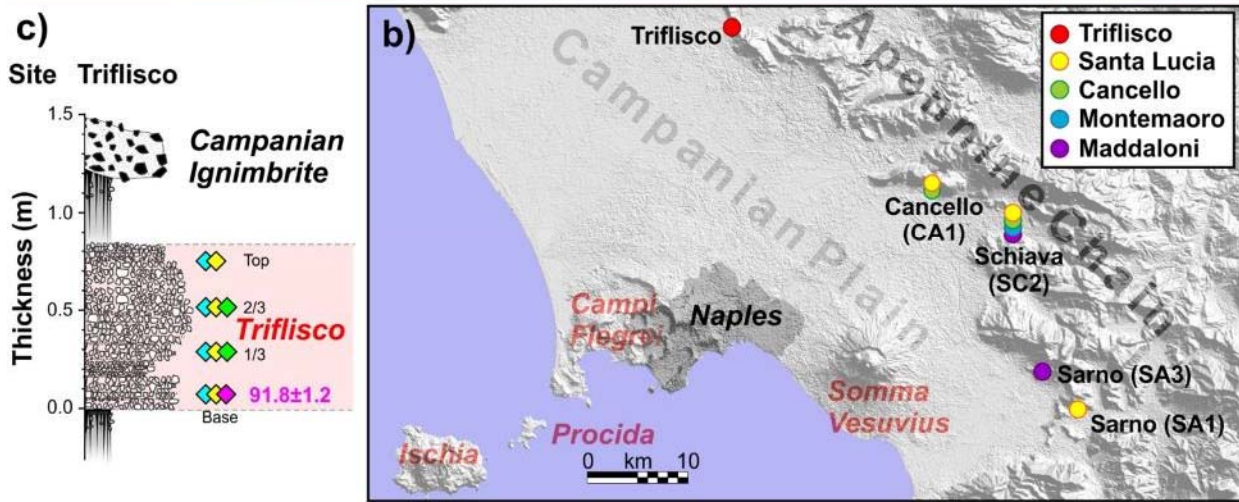
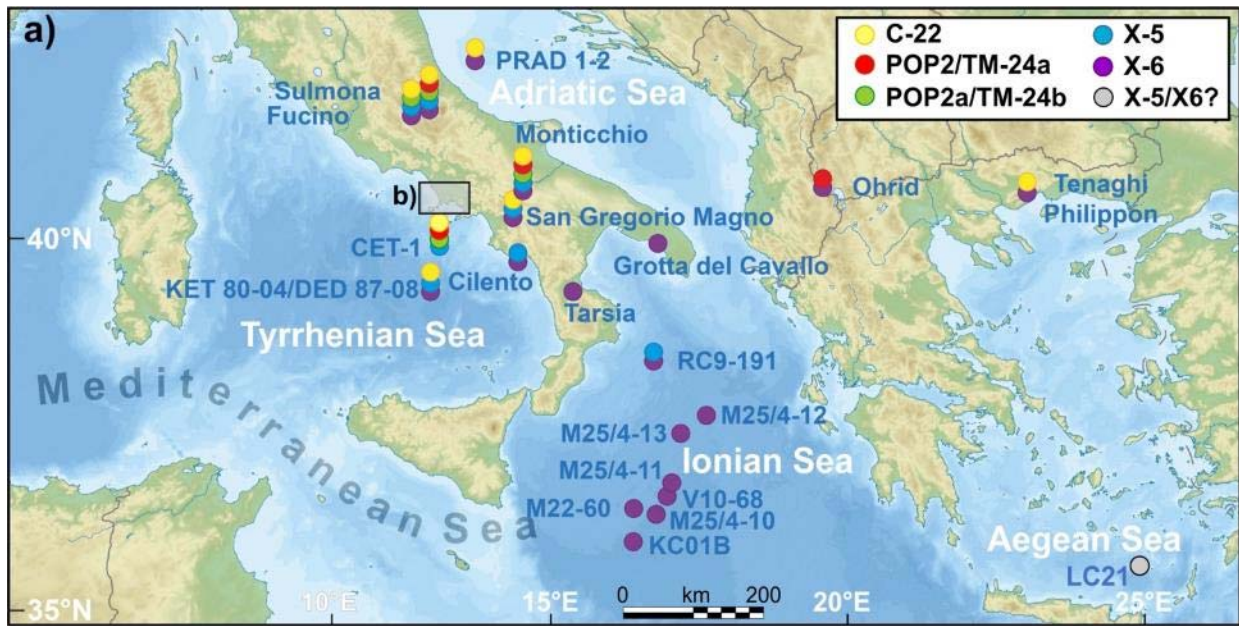
96

97 **Table 1.** Main Mediterranean tephrostratigraphic records documenting the occurrence of the MIS 5 Neapolitan-like tephra.

98

Site/area	Ionian Sea	Tyrrhenian Sea	Lago Grande di Monticchio	Sulmona Basin	Fucino Basin
Reference	Keller et al. (1978)	Paterne et al. (1986, 1988); Petrosino et al. (2016)	Wulf et al. (2004, 2012)	Giaccio et al. (2012); Regattieri et al. (2015, 2017)	Giaccio et al. (2017a)
		C-22	TM-23-11	POP-1	TF-10
		CET1-crypto 12/14	TM-24a	POP-2	
		CET1-crypto 15	TM-24b	POP-2A	TF-11
	X-5	C-27	TM-25	POP-3	TF-12
	X-6	C-31	TM-27	POP-4	TF-13

99



100
101
102
103
104
105

Figure 1. Reference maps and stratigraphic logs of the investigated sections. a) Central Mediterranean sedimentary successions containing the MIS 5 tephra markers investigated in this study. b) Digital Elevation Map (DEM) of the Campanian Plain with location of the Neapolitan volcanoes and the investigated pyroclastic successions (Cancelli-SEMAC Quarry, CA1; Schiava-Masseria Montemaoro Quarry, SC2; Sarno-Tre Valloni, SA1; Sarno-Pian della Colla, SA3). c) Stratigraphic logs of the investigated pyroclastic units showing the distribution of the analysed samples and the type of the performed analysis.

106
107

2. Geological setting: The Neapolitan volcanoes

108 The Neapolitan volcanoes comprise Campi Flegrei, Ischia and Procida islands and Somma-Vesuvius (Fig.
109 1). The Campi Flegrei volcanic field was the site of the most intense activity among the four Neapolitan
110 volcanoes, as well as in the whole Mediterranean area. Three main eruptions occurred in this volcanic area,
111 i.e., the Campanian Ignimbrite (CI; 39.85 ± 0.14 ka; [Giaccio et al., 2017b](#)), the Masseria del Monte Tuff (MdMT;
112 29.3 ± 0.7 ka; [Albert et al., 2015, 2019](#)), and the Neapolitan Yellow Tuff (NYT; 14.5 ± 0.4 ka; [Deino et al., 2004](#);
113 [Galli et al., 2017](#)) caldera-forming eruptions. Overall, while there is quite satisfactory knowledge on the activity
114 occurred in-between and after these three main events, especially that following the NYT (e.g., [Smith et al.,](#)
115 [2011](#)), the eruptive history preceding the CI is still poorly resolved, being documented only by deposits
116 sporadically exposed outside the caldera and dated back to ~ 80 ka (e.g., [Pappalardo et al., 1999](#); [Scarpati et](#)
117 [al., 2013](#)). Far from the Campi Flegrei volcanic area, several pyroclastic units documenting explosive activity
118 in the Campania region can be dated as back as 290 ka ([De Vivo et al., 2001](#); [Rolandi et al., 2003](#)). This older
119 activity is however referred to the so-called Campanian Volcanic Zone ([Rolandi et al., 2003](#)), i.e., a
120 hypothesized diffuse, regional volcanism not related to the present Campi Flegrei source area.

121 Volcanic activity at Ischia Island, off the Naples gulf (Fig. 1b), is documented as back as 150 ka, which is the
122 age of the oldest exposed deposits, and up to historical times (e.g., [Poli et al., 1987](#)). The activity of Ischia is
123 subdivided in five stages (i.e., >150 -75 ka; 75-55 ka; 55-33 ka; 28-12 ka; 12 ka-1302 CE), characterised by
124 different eruptive styles and types of products (e.g., [Poli et al., 1987](#); [Brown et al., 2008](#)). The third stage of
125 activity (55-33 ka) included several explosive events, following the largest 55 ka Monte Epomeo Green Tuff
126 eruption (MEGT; [Poli et al., 1987](#)), recognized in the Mediterranean region as the Y-7 tephra marker horizon
127 (e.g., [Tomlinson et al., 2014](#)), although this attribution has been recently questioned ([D'Antonio et al., 2021](#)).

128 The Island of Procida, located between Ischia Island and Campi Flegrei (Fig. 1b), was active over a period of
129 ~ 60 kyr, between ~ 80 ka and $23,624 \pm 330$ cal yr BP (e.g., [De Astis et al., 2004](#); [Morabito et al., 2014](#)). Its
130 activity originated from five eruptive centres, i.e. Vivara, Terra Murata, Pozzo Vecchio, Fiumicello, and
131 Solchiaro ([Rosi et al., 1988a, 1988b](#)) and is documented by pyroclastic deposits and lava dome interbedded
132 with Campi Flegrei and Ischia units, which acts as stratigraphic, chronological markers (e.g., [Morabito et al.,](#)
133 [2014](#)).

134 The Somma-Vesuvius stratovolcano, east of the Naples metropolitan area (Fig. 1b), has completely grown on
135 the products of the CI eruption (e.g., [Santacroce and Sbrana, 2003](#)), and thus it is younger than 40 ka. Its
136 activity is subdivided in three main stages: (i) the pre-Mercato eruption stage (ca. 35-9 ka), (ii) the stage

137 between Mercato and the infamous AD 79 Pompeii eruption (ca. 9 ka-79 CE) and (iii) the stage following the
 138 Pompeii eruption until present (i.e., last historical eruption of 1944 CE). These three stages differ from one
 139 another in terms of either the frequency of the related inter-Plinian eruptive episodes (e.g., [Andronico and](#)
 140 [Cioni, 2002](#)) or the silica undersaturation degree, both increasing over the time ([Santacroce et al., 2008](#)).

141

142 3. Methods

143 3.1. Sample selection

144 For the present study, we used samples collected from 4 eruptive units out of the 14 pre-CI eruption
 145 deposits recognised by [Di Vito et al. \(2008\)](#) in the Campanian Plain ([Fig. 1b](#)). They are, from bottom to top,
 146 SC2-a (hereafter Maddaloni), SC2-b (hereafter Montemaoro), CA1-a (hereafter Cancelli), and Santa Lucia
 147 ([Table 2](#); [Fig. 1c](#)). However, new analysis for the Montemaoro unit was not possible due to unavailability of
 148 the sample previously collected by [Di Vito et al. \(2008\)](#) and the inaccessibility of the outcrop during the new
 149 field investigations. The list of the investigated units is integrated with the fall deposit outcropping near the
 150 Triflisco village, at the edge of the Campanian Plain, here labelled Triflisco ([Fig. 1b-c](#)). Moreover, the isotopic
 151 characterisation has been performed also on samples CIL1 and CIL2 from the Cilento Coast being
 152 representative for the X5 and X6 stratigraphic markers ([Giaccio et al., 2012](#)).

153

154 **Table 2.** Location and data summary of the investigated units.

Units	Locality	Sample source	Coordinates	Sample/sub-units	Analysis			
					Major elements (EMPA)	Trace elements (LA-ICP-MS)	Sr-Nd isotopes	⁴⁰ Ar/ ³⁹ Ar age
Triflisco	Triflisco	This study	41°08'14" N 14°15'12" E	TRIF-Top	Y	Y	-	-
				TRIF-2/3	Y	Y	Y	-
				TRIF-1/3	Y	Y	Y	-
				TRIF-Base	Y	Y	-	Y
Santa Lucia (Santa Lucia)	Schiava, Masseria Montemaoro Quarry (SC2)	Di Vito et al. (2008)	40°56'39" N 14°33'56" E	ZS97-9	Y	Y	-	-
				ZS97-10	Y	Y	Y	Y
				ZS97-272	Y	Y	-	-
				ZS97-273	Y	Y	-	-
				ZS97-28	Y	Y	Y	-
Cancelli (CA1-a)	Sarno, Tre Valloni (SA1)	Di Vito et al. (2008)	40°49'03" N 14°38'06" E	ZS97-39	Y	Y	-	-
				ZS97-27	Y	-	-	-
Cancelli (CA1-a)	Schiava, Masseria Montemaoro Quarry (SC2)	Di Vito et al. (2008)	40°56'39" N 14°33'56" E	AS96-400	Y	Y	-	Y
				ZS97-8	Y	Y	-	-
Montemaoro (SC2-b)	Schiava, Masseria Montemaoro Quarry (SC2)	Di Vito et al. (2008)	40°56'39" N 14°33'56" E	SC2-b	-	-	-	-
Maddaloni (SC2-a)	Schiava, Masseria Montemaoro Quarry (SC2)	Di Vito et al. (2008)	40°56'39" N 14°33'56" E	ZS97-3	Y	Y	-	-
				Sarno, Pian della Colla (SA3)	40°48'44" N 14°39'31" E	ZS97-286	Y	Y
CIL1	Cilento Coast	Giaccio et al. (2012)	40°03'24" N 15°17'02" E	CIL1	Y ¹	-	Y	-
CIL2				CIL2	Y ¹	-	Y	-

155 "Y": type of analysis performed on the sample. "-": type analysis not performed on the sample. Literature data source: ¹ = [Giaccio et al.](#)
156 [\(2012\)](#).
157

158 3.2. Volcanic glass characterisation

159 3.2.1. Sample preparation

160 The samples selected for the major and trace glass composition ([Fig. 1c](#); [Table 2](#)) were wet sieved
161 with tap water through a series of sieves with decreasing mesh openings. All fractions were successively oven-
162 dried at 100°C until completely dry. For major element analysis, selected fractions of 60-250 µm were mounted
163 on 29 x 49 mm glass slides, embedded in epoxy resin, progressively ground to a thickness of 60-100 µm and
164 finally polished to be analysed with the electron microprobe. For trace element analysis, selected samples
165 were embedded in epoxy resin and successively polished.

166

167 3.2.2. Electron probe micro analyser (EPMA)

168 Glass shards and (micro-)pumice fragments were analysed by single-shard major element chemical
169 analysis using the electron probe micro analyser (EPMA). Analysis was first performed with a Jeol JXA-850F
170 equipped with five wave dispersive spectrometers (WDS), installed at the Institute of Petrology and Structural
171 Geology, Charles University of Prague (Prague, Czech Republic). The machine operated at 15 kV accelerating
172 voltage, 10 nA beam current and 10 µm defocused beam to limit alkali loss. Element counting times were of
173 20 s for all elements, except for Na, K, and S, for which counting times of 10 s (Na and K) and 30 s (S) were
174 employed respectively. For all measurements, the F content was always below the detection limit of the
175 machine. Standards for calibration were quartz (Si), corundum (Al), rutile (Ti), magnetite (Fe), periclase (Mg),
176 rhodonite (Mn), albite (Na), sanidine (K), diopside (Ca), apatite (P and F), tugtupite (Cl) and anhydrite (S). The
177 secondary standards GOR128-G ([Jochum et al., 2006](#)) and CFA47 ([Marianelli and Sbrana, 1998](#)) were
178 analysed at the beginning of each microprobe session for a total of one point each to evaluate analysis
179 accuracy.

180 Further WDS analyses were carried out at the Dipartimento di Scienze della Terra, Università degli Studi di
181 Firenze (Florence, Italy), with a Jeol Superprobe JXA-8230 equipped with five-WDS spectrometers. Operating
182 conditions were set to 15 kV accelerating voltage, 10 nA beam current and 10 µm defocused beam diameter
183 to limit Na mobilisation. Element counting times were 15 s for all elements except for Na (10s), F (20s), S
184 (30s), Mn, P and Cl (40s). Albite (Si and Na), ilmenite (Ti and Fe), plagioclase (Al), bustamite (Mn), olivine
185 (Mg), diopside (Ca), sanidine (K), apatite (P), fluorite (F), tugtupite (Cl) and celestine (S) were used as internal
186 standards. The accuracy of the measurements was assessed using the glass secondary standards GOR128-

187 G, ATHO-G and StHs6/80-G (Jochum et al., 2006), Lipari ID3506 (Kuehn et al., 2011), Scapolite NMNH, and
188 CFA47 (Marianelli and Sbrana, 1998).

189 For both analytical facilities, the ZAF method was used for matrix effect correction. We adopted 93 wt% as a
190 threshold for the measured totals. All compositional data are shown as oxide weight percentages (wt%) in the
191 TAS and bi-plots diagrams, with total iron measured as FeO, and normalised to 100% on a volatile-free basis
192 for correlation purposes. Collected data and secondary standards measurements are all reported in
193 Supplementary Materials-1.

194

195 3.2.3. *Laser Ablation Inductively Coupled Plasma Mass Spectrometry (LA-ICP-MS)*

196 Trace element analyses were conducted on volcanic glasses from the Triflisco, Santa Lucia, Canello,
197 and Maddaloni units. The analyses were performed using an Agilent 8900 triple quadrupole ICP-MS (ICP-
198 QQQ) coupled to a Resonetics 193nm ArF excimer laser-ablation device at the Department of Earth Sciences,
199 Royal Holloway, University of London. Full analytical procedures used for volcanic glass analysis follow those
200 reported in Tomlinson et al. (2010). Crater sizes of 20, 25 and 34 μm were used depending on the sample
201 vesicularity and/or size of glass surfaces available for analysis. The repetition rate was 5 Hz, with a count time
202 of 40 s on the sample, and 40 s on the gas blank to allow the subtraction of the background signal. Typically,
203 blocks of eight glass shards and one MPI-DING reference glass were bracketed by the NIST612 glass adopted
204 as the calibration standard. The internal standard applied was ^{29}Si (determined by EMP-WDS analysis). In
205 addition, MPI-DING reference glasses were used to monitor analytical accuracy (Jochum et al., 2006). LA-
206 ICP-MS data reduction was performed in Microsoft Excel, as outlined in Tomlinson et al. (2010). Accuracies
207 of LA-ICP-MS analyses of the MPI-DING reference glasses, ATHO-G and StHs6/80-G, were typically $\leq 5\%$
208 for the majority of elements measured. Tephra and standard measurements are all provided in Supplementary
209 Materials-1. Data averages reported in the text are accompanied by a ± 2 standard deviation (2 s.d.), whilst
210 error bars in the plots are typically smaller than the data symbols.

211

212 3.2.4. *Sr and Nd isotopes*

213 $^{87}\text{Sr}/^{86}\text{Sr}$ and $^{143}\text{Nd}/^{144}\text{Nd}$ isotope ratios have been determined on two samples from the Santa Lucia
214 and one from Maddaloni units (i.e., ZS97-10 and ZS97-28, and ZS97-286 respectively) previously investigated
215 by Di Vito et al. (2008), on two samples from the Triflisco unit (i.e., TRIF 1/3 and TRIF 2/3) and on the CIL1
216 and CIL2 units from the Cilento Coast (Giaccio et al. 2012; Fig. 1c; Table 2). Measurements have been
217 performed either on the glasses (pumices) and/or crystals (pyroxene or feldspar). $^{143}\text{Nd}/^{144}\text{Nd}$ measurement

218 were performed on the glass fraction of samples from Triflisco, Santa Lucia (ZS97-10) and Maddaloni (ZS97-
219 286) units. The different fractions were handpicked under a binocular microscope. Among all the available
220 glass shards/pumices the most homogeneous in colour, and visibly poorly affected by secondary alteration,
221 were selected for isotope analyses. Feldspar and pyroxene crystals were handpicked avoiding those
222 characterised by the presence of glass rinds attached on their surfaces.

223 Before chemical dissolution, glass shards/pumices were acid leached three to five times to reduce as much
224 as possible the alteration effects. The leaching procedure was prolonged until the acid solution became light-
225 yellow in colour. Leaching was carried out each time by placing the beakers containing samples and high purity
226 6N HCl on a hot plate for 10 min. During each leaching step and after the final leaching, samples were rinsed
227 with Milli-Q® H₂O. Feldspar and pyroxene were cleaned with Milli-Q® H₂O for 10 min. in an ultrasonic bath.
228 Dissolution was obtained with high-purity HF–HNO₃–HCl mixtures. Sr and Nd were separated from the matrix
229 through conventional ion-exchange procedures. Sr and Nd isotopic compositions were determined in a static
230 mode by thermal ionisation mass spectrometry (TIMS) using a Thermo Finnigan Triton TI® mass spectrometer
231 equipped with one fixed and six adjustable Faraday cups. Average 2σ mean, i.e., the standard error with N =
232 180, was better than ± 9x10⁻⁶ for Sr, and better than ± 7x10⁻⁶ for Nd measurements. The mean measured
233 values of ⁸⁷Sr/⁸⁶Sr for the NIST-SRM 987 standard and ¹⁴³Nd/¹⁴⁴Nd for the La Jolla standard were 0.710261 ±
234 0.000021 (2σ, N = 169) and 0.511845 ± 0.000010 (2σ, N = 55), respectively; external reproducibility (2σ)
235 during the period of measurements was calculated according to [Goldstein et al. \(2003\)](#). Measured ⁸⁷Sr/⁸⁶Sr
236 ratios were normalized for within-run isotopic fractionation to ⁸⁶Sr/⁸⁸Sr = 0.1194, and ¹⁴⁶Nd/¹⁴⁴Nd = 0.7219. The
237 final, measured isotope ratio values were normalized to the recommended values of the NIST SRM 987
238 (⁸⁷Sr/⁸⁶Sr = 0.71025) and La Jolla (¹⁴³Nd/¹⁴⁴Nd = 0.51185) standards, respectively. Chemistry processing and
239 isotope analyses were performed at the Radiogenic Isotope Laboratory (RIL) of the Istituto Nazionale di
240 Geofisica e Vulcanologia, Osservatorio Vesuviano, and the full analytical dataset is reported in Supplementary
241 Materials-2.

242

243 3.2.5. ⁴⁰Ar/³⁹Ar dating

244 The ⁴⁰Ar/³⁹Ar ages were obtained at the Laboratoire des Sciences du Climat et de l'Environnement
245 (CEA, CNRS UMR 8212, Gif-sur-Yvette, France) dating facility. Fresh and transparent K-rich feldspars were
246 extracted from Triflisco, Santa Lucia, Canello and Maddaloni samples. After being washed in distilled water,
247 transparent K-feldspars (500-630 μm) without any visible inclusions were handpicked under a binocular and
248 used for dating these four pyroclastic units.

249 Between 20 and 30 crystals for each sample were irradiated in the Cd-lined, in core CLICIT facility of the
250 Oregon State University TRIGA reactor for 2 h (IRR. CO-007) for Triflisco and 1 h in the same reactor (IRR.
251 CO-009) for Santa Lucia, Canello, and Maddaloni. Interference corrections were based on the nucleogenic
252 production ratios given in [Balbas et al. \(2016\)](#). After irradiation, individual crystal for each tephra layers were
253 transferred into a copper 133 pits sample holder placed into a differential vacuum Teledyne Cetac window
254 connected to a home designed compact extraction line. Minerals were fused one by one using a 100W
255 Teledyne Cetac CO₂ laser during 15s at 2.5 W. Before fusion, each crystal underwent a 10s long sweeping at
256 0.3W to remove unwanted gas potentially trapped on the crystals surface and fractures. Extracted gases were
257 firstly purified by a SAES GP 50 cold getter for 90s and then for 230s by two hot SAES GP 50 getters. The
258 five Argon isotopes (i.e., ⁴⁰Ar, ³⁹Ar, ³⁸Ar, ³⁷Ar and ³⁶Ar) were measured using a multicollector NGX 600 mass
259 spectrometer equipped with 9 ATONA® amplifiers array and an electron multiplier. More technical
260 specifications regarding the NGX 600 ATONA detector array are presented in detail in [Cox et al. \(2020\)](#). ⁴⁰Ar,
261 ³⁹Ar, ³⁸Ar, and ³⁶Ar isotopes were collected simultaneously while the ³⁷Ar was measured in a second time. In
262 the first run, ⁴⁰Ar, ³⁹Ar and ³⁸Ar were measured simultaneously on 3 ATONA® amplifiers and ³⁶Ar on the
263 electron multiplier. Following this first run the ³⁷Ar was measured alone using the electron multiplier. Each
264 isotope measurement corresponds to 15 cycles of 20-seconds integration time. Peak intensity data were
265 reduced using ArArCALC V2.4 ([Koppers, 2002](#)). Neutron fluence J factor was calculated using co-irradiated
266 Alder Creek sanidine standard ACs-2 associated to an age of 1.1891 Ma ([Niespolo et al., 2017](#)) according to
267 the K total decay constant of [Renne et al. \(2011\)](#) ($\lambda_{e.c.} = (0.5757 \pm 0.016) \times 10^{-10} \text{ yr}^{-1}$ and $\lambda_{\beta^-} = (4.9548 \pm 0.013)$
268 $\times 10^{-10} \text{ yr}^{-1}$). To determine the neutron flux for each sample we used at least 6 flux monitor crystals coming
269 from pits framing the samples in each irradiation disk. J-values are of $0.00056080 \pm 0.00000062$ (Triflisco
270 [Base]); $0.00028350 \pm 0.00000023$ (Santa Lucia [ZS97-10]); $0.00028340 \pm 0.00000028$ (Canello [AS96-400]);
271 $0.00028340 \pm 0.00000020$ (Maddaloni [ZS97-286]). To verify the detectors linearity, mass discrimination was
272 monitored by analysis of at least 60 air shots of various beam sizes ranging from $5.0 \cdot 10^{-3}$ up to $2.0 \cdot 10^{-2}$ V (1
273 to 4 air shots). About 15 air shots analyses are performed every day. These measurements are done
274 automatically during the nights before and after the unknown measurements. Discrimination is calculated
275 according the ⁴⁰Ar/³⁶Ar ratio of 298.56 ([Lee et al., 2006](#)). Procedural blank measurements were achieved after
276 every two to three unknowns. For typical 5 min time blank backgrounds are between 2.5 and $4.0 \cdot 10^{-4}$ V for ⁴⁰Ar
277 and 60 to 90 cps for ³⁶Ar (about 1.0 - $1.3 \cdot 10^{-6}$ V equivalent). Full analytical data for each sample can be found
278 in Supplementary Materials-3.

279

280 4. Results

281 4.1. Stratigraphy

282 Most samples investigated in this study refer to the pyroclastic units already described in [Di Vito et al.](#)
283 [\(2008\)](#), to which the reader is referred for the lithostratigraphic details. They generally consist in dm-thick fallout
284 deposits made up of either pumice lapilli or coarse ash ([Fig. 1c](#)). At the site “Schiava” (SC2 in [Fig. 1b](#)) all the
285 four previously investigated units, i.e., Maddaloni, Montemaoro, Canello and Santa Lucia, occur as distinct
286 eruptive units separated by either paleosols, epiclastic deposits or unconformity bounding surfaces.
287 The newly recognised Triflisco unit ([Fig. 1b](#)), consists in an 80 cm-thick fallout deposit made up of moderately
288 sorted, white-pinkish and well-vesicular pumice lapilli (max Φ 3 cm) with intervening coarse ash layers.
289 Accidental lithics are scant ([Fig. 1c](#)). The Triflisco unit overlies a paleosol and at the top, in turn, it is capped
290 by a thick reddish paleosol on which lays a greyish pyroclastic flow deposit that we attribute to the CI ([Fig. 1c](#)).
291 Thus, our interpretation differs from previous ones that correlated the pumice fall at this locality to the CI Plinian
292 fall exposed elsewhere ([Civetta et al., 1997](#); [Fanara et al., 2015](#)).

293

294 4.2. Major and minor element volcanic glass chemistry

295 All samples analysed in this study have a dominant composition overlapping the boundary between
296 phonolite and trachyte fields ([Fig. 2a](#)) of the *Total alkali vs Silica* (TAS, [Le Maitre et al., 2002](#)) classification
297 diagram. Mean compositions are reported at 2σ (2 standard deviation) error.

298 **Triflisco unit.** It is made up by four sub-units ([Fig. 1c](#)) with a relatively homogeneous composition. The majority
299 of the data straddle the boundary between trachyte and phonolite fields (SiO_2 content of 59.5 ± 0.9 wt%, and
300 alkali sum of 12.8 ± 1.0 wt%), depicting a trend within the trachyte field with decreasing alkali negatively
301 correlated with a small increase in silica; [Fig. 2a-b](#)). The CaO/FeO values are < 1 (0.8 ± 0.1) and the Cl content
302 is 0.6 ± 0.1 wt% for all sub-units ([Fig. 2c](#)). Glasses display a High Alkali Ratio (HAR), with $\text{K}_2\text{O}/\text{Na}_2\text{O}$ generally
303 > 2 and up to 3.08 ([Fig. 2d](#)). There is no appreciable chemical variation from the lowermost (Triflisco Base) to
304 the uppermost (Triflisco Top) sub-units.

305 **Santa Lucia unit.** The glass of this unit, analysed in six samples ([Fig. 1c](#); [Table 2](#)), is characterised by the
306 most heterogeneous composition among those analysed, although mainly phonolitic, with a mean SiO_2 content
307 of 59.0 ± 2 wt%, and an alkali sum of 12.8 ± 1 wt% ([Fig. 2a-b](#)). The CaO/FeO ratio is ≤ 1 (mean of 0.9 ± 0.1)
308 and the Cl content is medium-high (0.6 ± 0.1 wt%; [Fig. 2c](#)). Santa Lucia glasses display a HAR typically ≥ 2 ,
309 with a mean $\text{K}_2\text{O}/\text{Na}_2\text{O}$ ratio of 2.1 ± 0.5 ([Fig. 2d](#)).

310 **Cancello unit.** Glasses from this unit are phonolitic-trachytic in composition, with a SiO₂ content of 60.9 ± 1.3
311 wt%, a mean alkali sum of 13.1 ± 0.9 wt% (Fig. 2a-b) and a HAR of 2.2 ± 0.6 (Fig. 2d). The CaO/FeO ratio
312 ranges between 0.7 and 1.0 and the Cl content between 0.5 and 0.7 wt% (Fig. 2c).

313 **Montemaoro unit.** As stated in the previous section, it was not possible to acquire new data for this unit. Thus,
314 for the purpose of this study, we rely on the available glass-EDS data from Di Vito et al. (2008). The
315 Montemaoro unit is mainly trachytic in composition with some points straddling the boundary with the phonolite
316 field, with silica and alkali sum content of c.a. 61 wt% and 13 wt%, respectively (Fig. 2a-b). The glasses display
317 a HAR, up to 2.5, with a CaO/FeO ratio of c.a. 0.7 (Fig. 2d), while Cl content was not determined.

318 **Maddaloni unit.** The glass of this unit, collected from the former SC2 and SA3 sections (Fig. 1; Table 2), is
319 characterised by a homogeneous SiO₂ content (mean 61.6 ± 0.5 wt%), with an alkali sum of 13.7 ± 0.6 wt%
320 (Fig. 2a-b). Respect to all the above-mentioned samples, Maddaloni glasses predominantly display a Low
321 Alkali Ratio (LAR), with K₂O/Na₂O typically ≤ 1.5 (0.9 ± 0.1; Fig. 2d), due to an almost equal content of K₂O
322 and Na₂O of ca. 7 wt%. In addition to a lower K₂O/Na₂O ratio, with respect to the other analysed units, the
323 glass of the Maddaloni pumices has noticeably lower CaO/FeO ratios (0.5 ± 0.1), whilst the Cl content is
324 appreciably higher, up to 1.1 wt% (Fig. 2c).

325

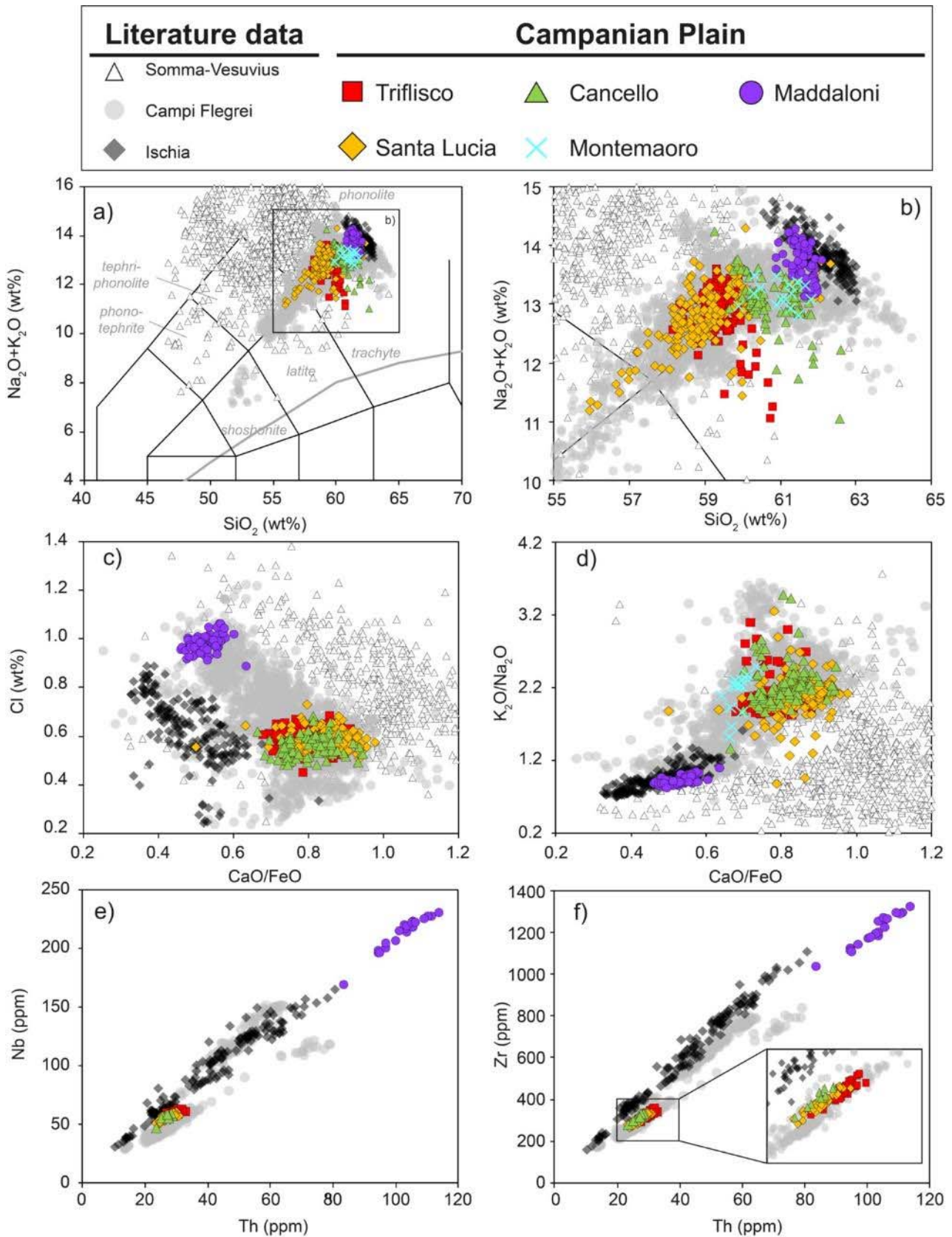
326 4.3. Trace element volcanic glass chemistry

327 The Triflisco eruption unit contains HAR glasses that are fairly homogeneous in terms of their
328 incompatible trace element contents (e.g., Th = 29.9 ± 2.9 ppm [Fig. 2e-f]; Nb = 59.2 ± 4.0 ppm [Fig. 2e]; Zr =
329 327 ± 31 ppm [Fig. 2f]) and ratios of other High Field Strength elements (HFSE) to Th remaining constant (e.g.,
330 Nb/Th = 2.0 ± 0.1; Zr/Th = 10.9 ± 0.5). Light Rare Earth Elements (LREE) are enriched relatively to the Heavy
331 Rare Earth Elements (HREE) with La/Yb = 27.9 ± 3.7.

332 The HAR Santa Lucia eruption products in the SC2, CA1 and SA1 sections (see Table 2) are compositionally
333 consistent and fairly homogeneous (e.g., Th = 27.1 ± 3.1 ppm; Nb = 55.8 ± 4.5 ppm [Fig. 2e]; Zr = 306 ± 29
334 ppm [Fig. 2f]; Rb = 307 ± 25 ppm; La = 77.9 ± 6.0 ppm) with constant HFSE/Th ratios (Nb/Th = 2.1 ± 0.1; Zr/Th
335 = 11.3 ± 0.5) and displaying LREE enrichment relatively to HREE (La/Yb = 27.7 ± 3.1).

336 The Cancello unit displays HAR glasses that are fairly homogeneous in composition (e.g., Th = 26.7 ± 3.0
337 ppm; Nb = 56.1 ± 7.0 ppm [Fig. 2e]; Zr = 316 ± 34 ppm [Fig. 2f]; La = 81.4 ± 8.3 ppm), with minor variation
338 relating to a single less enriched analysis. HFSE to Th ratios remain constant within the Cancello glasses
339 (Nb/Th = 2.1 ± 0.2; Zr/Th = 11.8 ± 0.4), and LREE are enriched relative to the HREE where La/Yb = 27.6 ±

340 3.4.



342
 343
 344
 345
 346
 347
 348
 349

Figure 2. Major and trace element compositions of the investigated medial Campanian Plain units in comparison with literature data of Ischia and Campi Flegrei volcanic systems. (a, b) *Total alkali vs silica* (TAS; [Le Maitre et al., 2002](#)), (c) *CaO/FeO vs Cl* classification diagram ([Giaccio et al., 2017a](#)), (d) *CaO/FeO vs K₂O/Na₂O*, (e) *Th vs Nb* (ppm) and (f) *Th vs Zr* (ppm). Glass-WDS data source: Triflisco, Santa Lucia, Canello and Maddaloni medial Campanian Plain units: this study; Somma-Vesuvius: [Santacroce et al. \(2008\)](#); Ischia: [Tomlinson et al. \(2014\)](#); Campi Flegrei: [Smith et al. \(2011, 2016\)](#), [Tomlinson et al. \(2012\)](#). Trace elements data source: Triflisco, Santa Lucia, Canello and Maddaloni medial Campanian Plain units: this study; Ischia: [Tomlinson et al. \(2014\)](#); Campi Flegrei ([Tomlinson et al., 2012](#)).

350 The LAR Maddaloni tephra shows variable incompatible trace element glasses compositions (e.g., Th = 84-
351 114 ppm; Nb = 169-231 ppm [Fig. 2e]; Zr = 1037-1319 ppm [Fig. 2f]) and displays far greater levels of
352 enrichment relative to the above mentioned HAR units (i.e., Triflisco, Santa Lucia and Canello; Fig. 2e-f).
353 HFSE/Th values remain constant within these glasses (Nb/Th = 2.1 ± 0.1 ; Zr/Th = 11.8 ± 0.4) and are entirely
354 consistent with the HAR samples from Triflisco, Santa Lucia and Canello deposits (Fig. 2e-f).

355

356 4.4. Sr and Nd isotopes

357 Whilst the $^{143}\text{Nd}/^{144}\text{Nd}$ isotopic ratios are homogeneous within the analytical error (c.a. 0.51250), the
358 $^{87}\text{Sr}/^{86}\text{Sr}$ ratios (Fig. 3a) range from 0.70687 and 0.70780 (glass from sample ZS97-286). The highest value is
359 possibly due to post-depositional alteration of the glass as suggested by the Sr isotope composition of the
360 embedded feldspar. Samples from Triflisco and Santa Lucia display similar and lower Sr isotope composition
361 (c.a. 0.7069) with respect to sample from Maddaloni unit. CIL1 and CIL2 are characterized by Sr isotope ratios
362 (from ca. 0.7071 to 0.7072) similar to that of the Maddaloni feldspar (from c.a. 0.7071). Figure 3 displays the
363 variations in terms of Sr-Nd isotope ratios compared with literature data.

364

365 4.5. $^{40}\text{Ar}/^{39}\text{Ar}$ ages

366 All $^{40}\text{Ar}/^{39}\text{Ar}$ results for individual tephra layers are presented as probability diagrams (Fig. 4). Weighted
367 mean age uncertainties are all reported at 2σ , including J uncertainty and were calculated using Isoplot 4.0
368 (Ludwig, 2001). For each sample, inverse isochrones have an atmospheric $^{40}\text{Ar}/^{36}\text{Ar}$ initial intercept with
369 uncertainties suggesting that dated crystals are without detectable excess argon. Full inverse isochrones
370 dataset can be found in Supplementary Materials-3.

371 **Triflisco (TRIF-Base)** - 13 single crystals were individually dated. Eleven out of thirteen crystals analysed
372 gave a similar age within uncertainties (Fig. 4a). The two other older crystals, one sanidine (~104 ka, red bar
373 in Fig. 4) and one plagioclase (~404 ka, not showed in Fig. 4; see Supplementary Materials-3) according to
374 their Ca/K ratio, are interpreted as xenocrysts. The main population of crystal interpreted as juvenile allows to
375 calculate a weighted mean age of 91.8 ± 1.2 ka (MSWD = 1.20, $p = 0.27$).

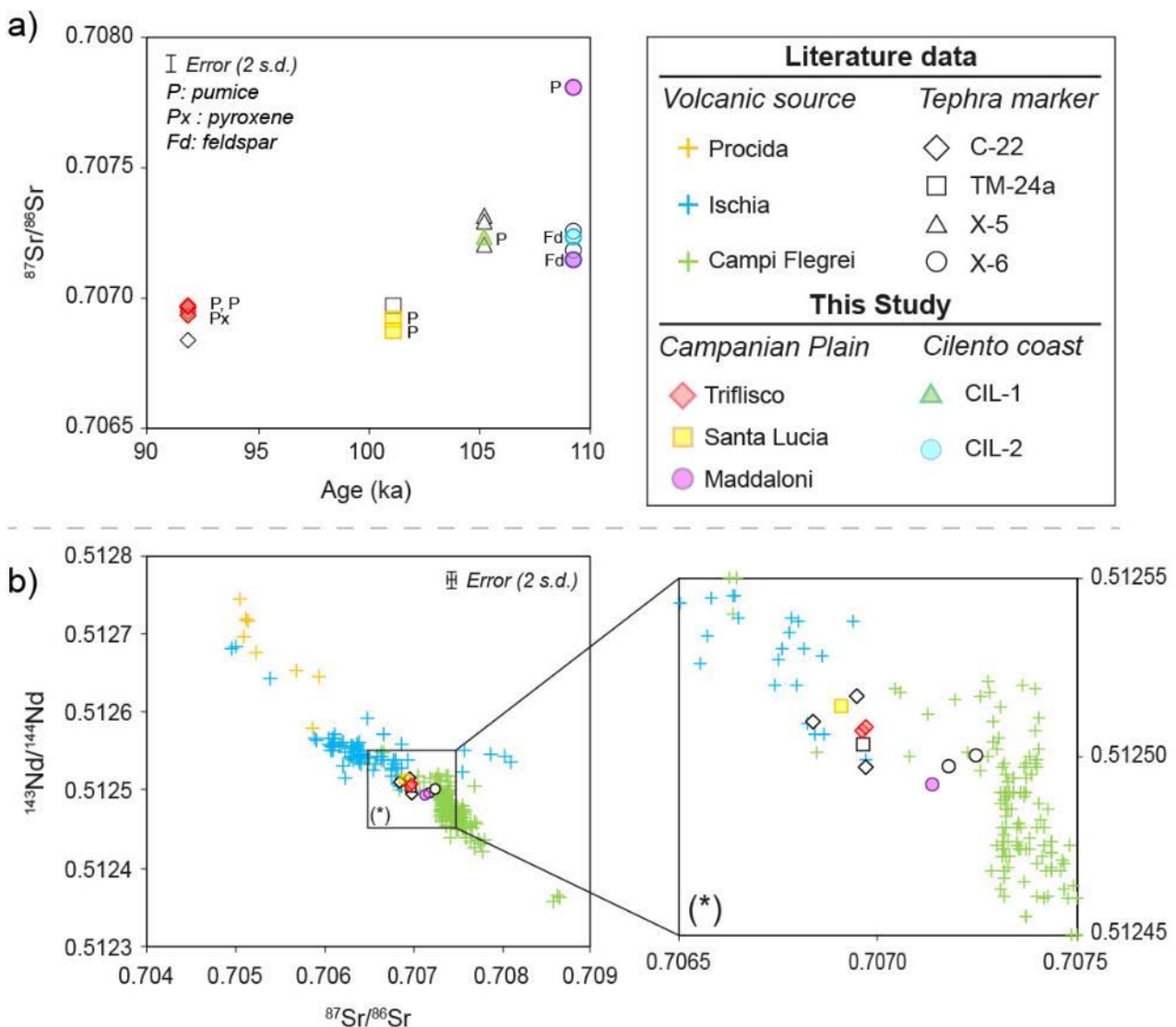
376 **Santa Lucia (ZS97-10)** - A total of 14 individual sanidine crystals were dated. The probability diagram is simple
377 (Fig. 4b) with one mode allowing to calculate a meaningful and precise weighted mean age of 101.2 ± 0.8 ka
378 (MSWD = 0.59, $p = 0.87$).

379 **Cancello (AS96-400)** - The probability diagram displays one single mode with no xenocrystal contamination
 380 (Fig. 4c). These crystals are interpreted as juvenile ones (12 crystals), allowing to calculate a precise weighted
 381 mean age of 102.5 ± 0.8 ka (MSWD = 0.58, $p = 0.85$).

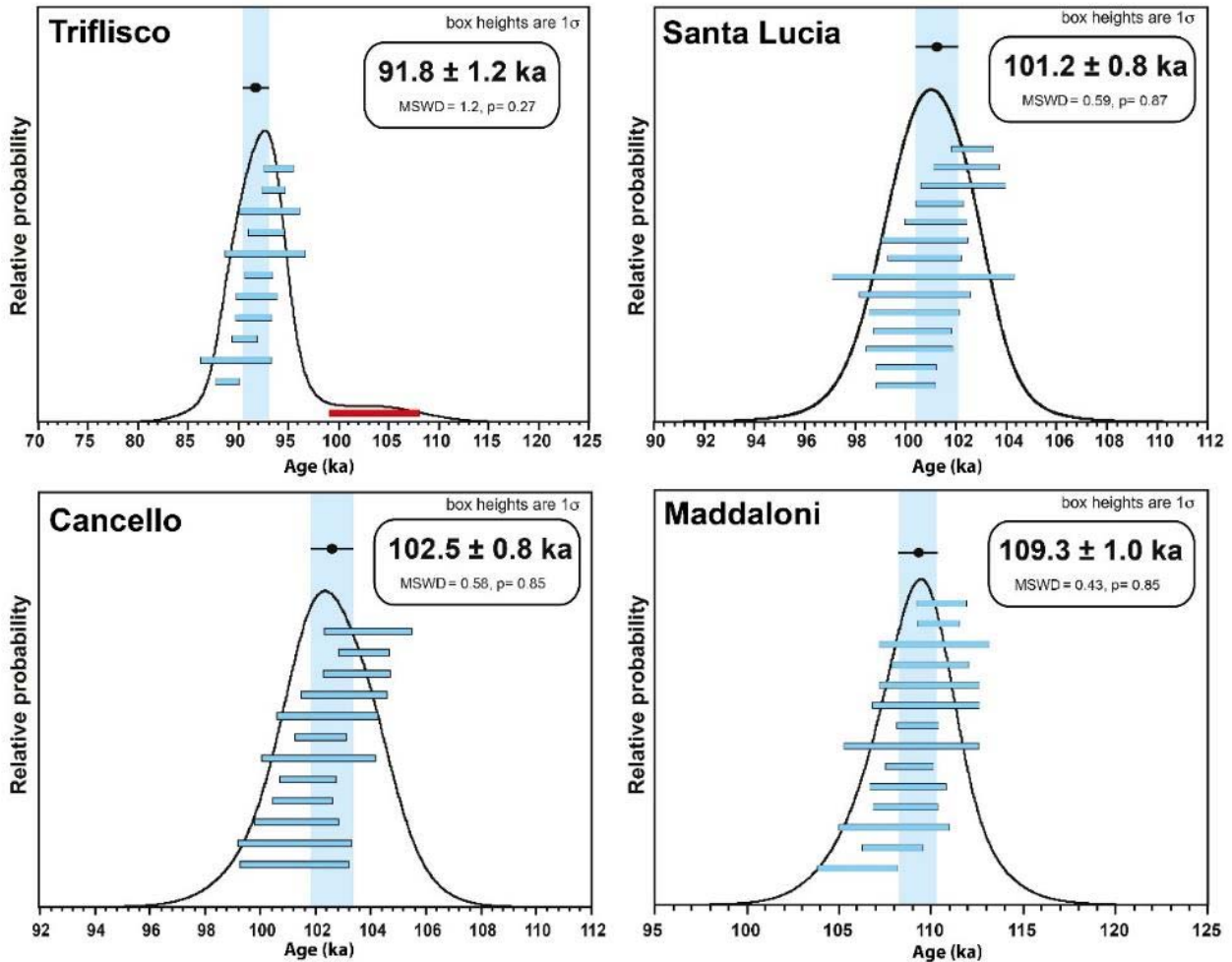
382 **Maddaloni (ZS97-286)** - 14 crystals were dated individually. All gave within uncertainty the same age resulting
 383 in a gaussian probability diagram (Fig. 4d). Using this very homogenous crystal population we calculated a
 384 weighted mean age of 109.3 ± 1.0 ka (MSWD = 0.43, $p = 0.96$).

385 While for Maddaloni we obtained the $^{40}\text{Ar}/^{39}\text{Ar}$ age of 109.3 ± 1.0 ka, the overlying Montemauro unit, which
 386 was not resampled or re-analysed in this work, was not dated.

387



388 **Figure 3.** Sr and Nd isotope ratios determined for the Triflisco, Santa Lucia and Maddaloni units from the Campanian Plain and CIL-1
 389 and CIL-2 tephra from the Cilento coast. In panel b the Sr isotope composition of the feldspar from the Maddaloni sample has been
 390 associated to the Nd isotope composition of its glass fraction, being the glass possibly affected by post depositional alteration. This latter
 391 did not modify the $^{143}\text{Nd}/^{144}\text{Nd}$, because the Nd is a less fluid mobile element. Tephra layers literature data source: **C-22**: POP-1 (Giaccio
 392 et al., 2012), TF-10 (Giaccio et al., 2017a), S14 (Petrosino et al., 2019); **TM-24a**: POP-2A (Giaccio et al., 2012); **X-5**: TF-12 (Giaccio et
 393 al., 2017a), S11 (Petrosino et al., 2019); **X-6** = TF-13 (Giaccio et al., 2017a), S10 (Petrosino et al., 2019). Literature data for Ischia, Procida
 394 and Campi Flegrei proximal deposits: Arienzo et al. (2009, 2010, 2015, 2016), Brown et al. (2014), Casalini et al. (2018), D'Antonio et al.
 395 (2007, 2013), Di Renzo et al. (2011), Pabst et al. (2007), Pelullo et al. (2020), Tonarini et al. (2009).



397

398

399

400

401

402

403

404

405

406

407

408

409

410

411

412

413

Figure 4. Age probability diagrams for the Triflisco, Santa Lucia, Canello and Maddaloni units. The light-blue and red horizontal bars are the single crystal ages with the uncertainty expressed at 1σ . Whilst the light-blue bars are included in the weighted mean age (vertical light-blue bars, 2σ uncertainty), the red ones are not included because statistically different and thus interpreted as ages of xenocrysts.

5. Discussion

5.1. Volcanic source of the Campanian Plain Units

All the investigated pyroclastic fall units occur in a range of 30-35 km to 55-60 km in the eastern quadrants from the Neapolitan volcanoes, including Campi Flegrei, Ischia, Procida and Somma-Vesuvius (Fig. 1b). Somma-Vesuvius can be reasonably excluded as a potential source since its oldest known activity is younger than Campanian Ignimbrite (i.e., < 40 ka; Santacrose et al., 2008) and thus incompatible with the 109-92 ka chronology obtained here for the Campanian Plain units. Also, in terms of glass chemical composition, the Somma-Vesuvius products appear incompatible due to the higher alkali sum at similar SiO_2 content (Fig. 2a-b), and the significantly higher CaO/FeO at same Cl content and alkali ratio (Fig. 2c-d). Procida island can also be excluded based on the Sr-Nd isotope compositions, which are clearly different from those of the Campanian Plain units (Fig. 3a-b). Among the two remaining potential sources for the investigated units (i.e., Campi Flegrei and Ischia), based on the lithostratigraphic and geochemical characteristics, as already argued

414 by [Di Vito et al. \(2008\)](#), the Campi Flegrei volcanic area is the most probable. In terms of major element glass
415 composition, although Campi Flegrei and Ischia products partially overlap, each of the two volcanic sources
416 show distinctive features in terms of oxide concentrations and ratios ([Fig. 2a-d](#)). This applies to four out of the
417 five investigated units (i.e., Triflisco, Santa Lucia, Canello, and Montemaoro), which unambiguously plot in
418 the compositional field of the Campi Flegrei glass because of the higher K_2O/Na_2O and CaO/FeO values with
419 respect to the Ischia products ([Fig. 2b-c](#)). Trace elements glass compositions also support the attribution of
420 the Triflisco, Santa Lucia and Canello units to the Campi Flegrei, for instance all these units show enrichment
421 in Zr that is diagnostic of the Campi Flegrei products and is slightly lower than that of the products typically
422 erupted at Ischia ([Fig. 2f](#)).

423 Owing to its distinctive K_2O/Na_2O and CaO/FeO values, which are lower than those of the most common
424 Campi Flegrei products ([Fig. 2c-d](#)), the source attribution of the Maddaloni unit is not so straightforward.
425 Indeed, CaO/FeO and K_2O/Na_2O ratios of Maddaloni unit partly overlap with those of Ischia ([Fig. 2b-c](#)).
426 However, using the CaO/FeO vs. Cl diagram, the glass composition of Maddaloni unit falls out of the Ischia
427 field and within the Campi Flegrei one, though, sporadically, the Campi Flegrei compositions can overrun the
428 typical Ischia one ([Fig. 2c](#)). Indeed, such chemical characteristics, i.e., LAR trachyte-phonolite with relatively
429 low CaO/FeO ratio, are also found in Campi Flegrei products (e.g., [Tomlinson et al., 2012](#)), notably in the Cl
430 ([Smith et al., 2016](#)) and some minor Campi Flegrei eruptions following the NYT caldera-forming eruption (e.g.,
431 Averno 2, Fondi di Baia, Monte Nuovo; [Smith et al., 2011](#)). Likewise, the Maddaloni unit can be attributed to
432 the Campi Flegrei and ascribed to this less common, LHR trachyte-phonolite compositional group of this
433 volcanic area. Incompatible trace element enrichment of the Maddaloni glasses exceeds that currently
434 recognised in the known products of Campi Flegrei and Ischia ([Fig. 2e-f](#)) making their use again less
435 conclusive. However, the lower Zr/Th ratios observed in the Maddaloni glasses are seemingly more akin to
436 those of Campi Flegrei, rather than to the higher values typically observed in the eruptive products of Ischia
437 spanning a period of intense explosive volcanism at ~40-80 ka ([Tomlinson et al., 2014](#)). More convincing, and
438 seemingly definitive, evidence to confirm Campi Flegrei as the source for the Maddaloni unit, is provided by
439 isotope data. Indeed, the Sr- and Nd-isotope compositions for the Maddaloni samples are positioned well
440 within the field of the Campi Flegrei ([Fig. 3a-b](#)).

441 In summary, the volcanological and sedimentological constraints, the acquired major and trace elements glass
442 composition, the geochronological and Sr- and Nd-isotope data consistently indicate that Campi Flegrei is the
443 most probable source for all the five investigated Campanian Plain units. This significantly extends back in
444 time the known explosive activity of this volcanic field, previously documented only up to ca. 80 ka ([Scarpati](#)

445 [et al., 2013](#)), or as far back as 290 ka (CVZ; [De Vivo et al., 2001](#); [Rolandi et al., 2003](#)). Regardless the precise
446 vent location, our data point to a frequent activity that took place within the Campi Flegrei volcanic area.
447 Specifically, we recognised five eruptions that, based on their lithological features in medial settings, can be
448 likely considered of Plinian intensity and magnitude. These occurred across approximately a 17 kyr time-
449 window, with recurrence times of a few thousands of years and in one case are barely more than 1 kyr (e.g.,
450 time elapsed between the 102.5 ± 0.8 ka Canello and the 101.2 ± 0.8 ka Santa Lucia eruptions).
451 Consequently, the period of 109-92 ka was characterized by a high frequency of moderate to large explosive
452 eruptions, i.e., an eruptive behaviour that has not been recognised within the more recent (i.e., post-CI) activity
453 of the Campi Flegrei volcano.

454

455 *5.2. Tephra correlations*

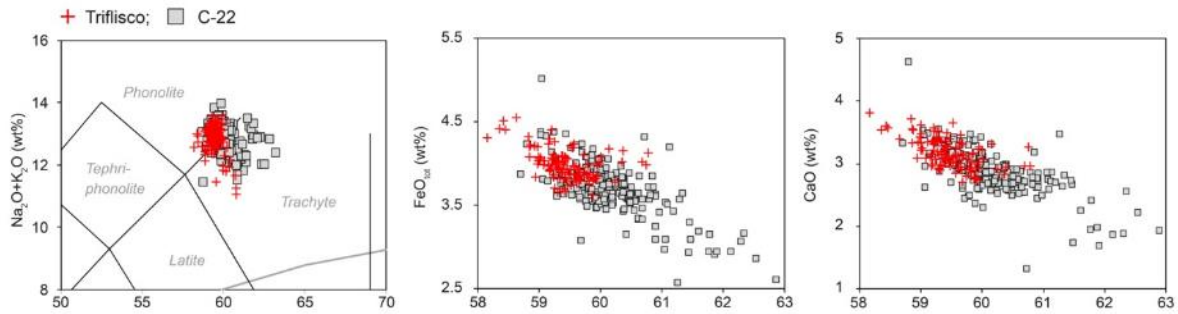
456 To correlate the investigated units of the Campanian Plain with MIS 5 Mediterranean tephra markers, we
457 refer to the Central Mediterranean tephrostratigraphic successions spanning this interval that (i) record in
458 stratigraphic order most MIS 5 tephra markers, (ii) have a good geochemical characterization of all tephra, (iii)
459 have a good radioisotopic or stratigraphic chronology, and (iv) have a good expression of the MIS 5 climate
460 variability, which enable a reliable assessment of the tephra climato-stratigraphic position.

461 These requisites are fully or partially met by (i) the rich tephrostratigraphic record of the Lago Grande di
462 Monticchio, southern Italy ([Fig. 1a](#)), located ca. 120 km east of the Neapolitan volcanoes – thus in an ideal
463 position for recording their explosive activity ([Wulf et al., 2004, 2012](#)) – and (ii) the Popoli MIS 5 succession,
464 in Sulmona Basin ([Fig. 1a](#)), where MIS 5 tephra were dated by $^{40}\text{Ar}/^{39}\text{Ar}$ method ([Giaccio et al., 2012](#); [Regattieri](#)
465 [et al., 2017](#)), allowing a direct, unambiguous comparison with the $^{40}\text{Ar}/^{39}\text{Ar}$ chronology here obtained for the
466 investigated Campanian Plain units.

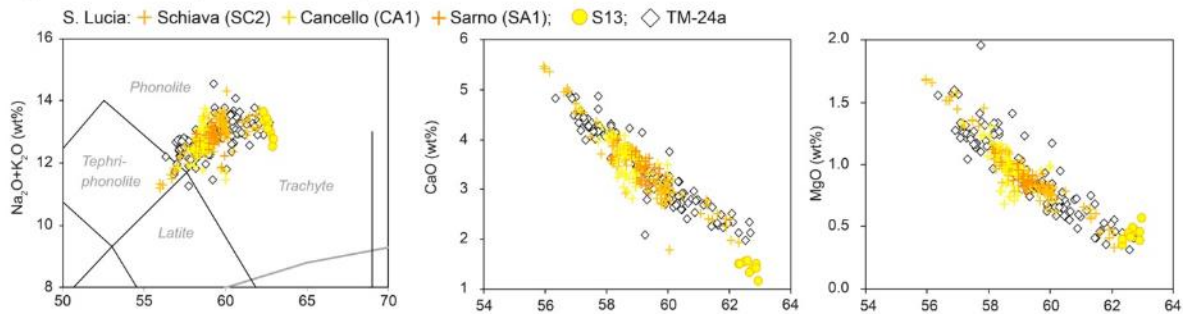
467

468 **Triflisco** - Both $^{40}\text{Ar}/^{39}\text{Ar}$ chronology and major elements ([Fig. 5a](#)) glass composition of Triflisco unit ($91.8 \pm$
469 1.4 ka) are fully consistent with those of the Sulmona tephra POP1 (92.1 ± 4.6 ka; [Giaccio et al., 2012](#)) that,
470 in turn, was correlated to the Monticchio tephra TM-23-11 ([Giaccio et al., 2012](#); [Fig. 5a](#)), dated at 95.18 ± 4.76
471 ka ([Wulf et al., 2012](#)). POP1/TM-23-11 was also correlated to the widespread C-22 tephra marker ([Giaccio et](#)
472 [al., 2012](#)) of the Tyrrhenian Sea tephra series ([Paterne et al., 1986, 1988](#)). The correlation of Triflisco with
473 POP1/TM-23-11/C-22 is supported also by incompatible trace element contents plotted against Th ([Fig. 6a](#)).
474 Furthermore, $^{87}\text{Sr}/^{86}\text{Sr}$ isotope ratios of Triflisco perfectly match literature values for the POP1/TM-23-11/C-22
475 tephra layers/markers ([Fig. 3a](#)), strengthening this correlation.

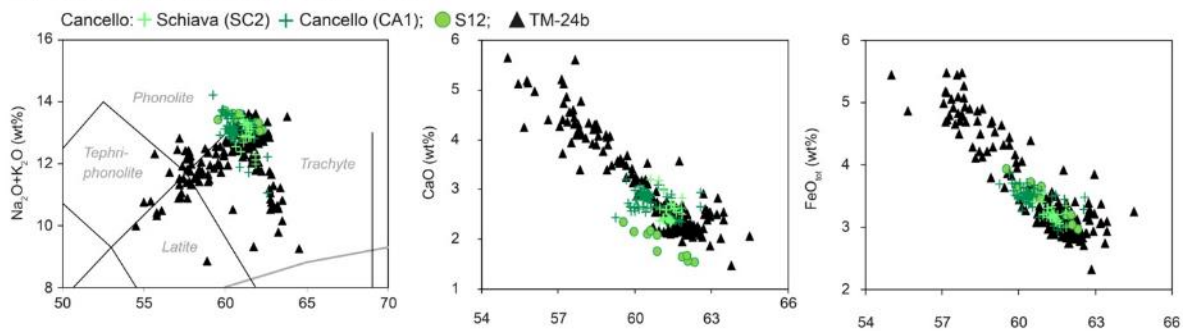
a) Triflisco (91.8 ± 1.2 ka) vs C-22



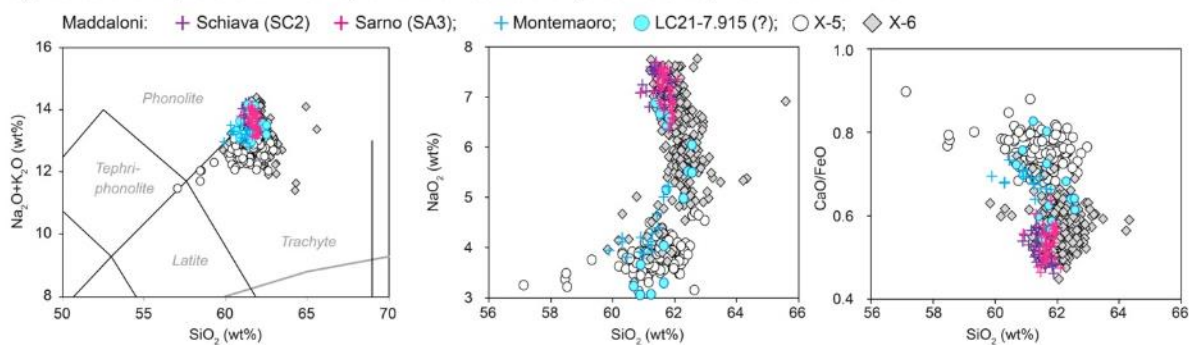
b) Santa Lucia (101.2 ± 0.8 ka) vs TM-24a



c) Cancellò (102.5 ± 0.8 ka) vs TM-24b



d) Maddaloni (109.3 ± 1.0 ka) and Montemauro (109-103 ka) vs X-6 and X-5



476

477

478

479

480

481

482

483

484

485

486

487

488

Figure 5. Major element bi-plots and ratios of Triflisco, Santa Lucia, Cancellò, Montemauro and Maddaloni units from the Campanian Plain in comparison with literature data. Literature EDS data source: SC2-b (Di Vito et al., 2008), S13, S12 (Munno and Petrosino, 2007). Literature glass-WDS data source: C-22 marker = TM-23-11 (Wulf et al., 2004), POP-1 (Giaccio et al., 2012), PRAD-2525 (Bourne et al., 2015), TF-10 (Giaccio et al., 2017a), TP05-25.195 (Wulf et al., 2018); TM-24a marker = TM-24a (Wulf et al., 2012), POP-2 (Regattieri et al., 2015); TM-24b marker = TM-24b (Wulf et al., 2012), POP-2A (Giaccio et al., 2012), OH-DP-0404 (Leicher et al., 2016), TF-11 (Giaccio et al., 2017a); X-5 marker = TM-25 (Wulf et al., 2012), POP-3, CIL-1 (Giaccio et al., 2012), LeS1 (Donato et al., 2016), TF-12 (Giaccio et al., 2017a), LC21-7.915 (Satow et al., 2015); X-6 marker = TM-27 (Wulf et al., 2012, 2018), CIL-2 (Giaccio et al., 2012), I-9 (Insinga et al., 2014), POP-4 (Regattieri et al., 2015), PRAD-2812 (Bourne et al., 2015), OH-DP-0435 (Leicher et al., 2016), Tarsia, LeS2 (Donato et al., 2016), TF-13 (Giaccio et al., 2017a), TP05-27.915 (Wulf et al., 2018), Cavallo-G (Zanchetta et al., 2018).

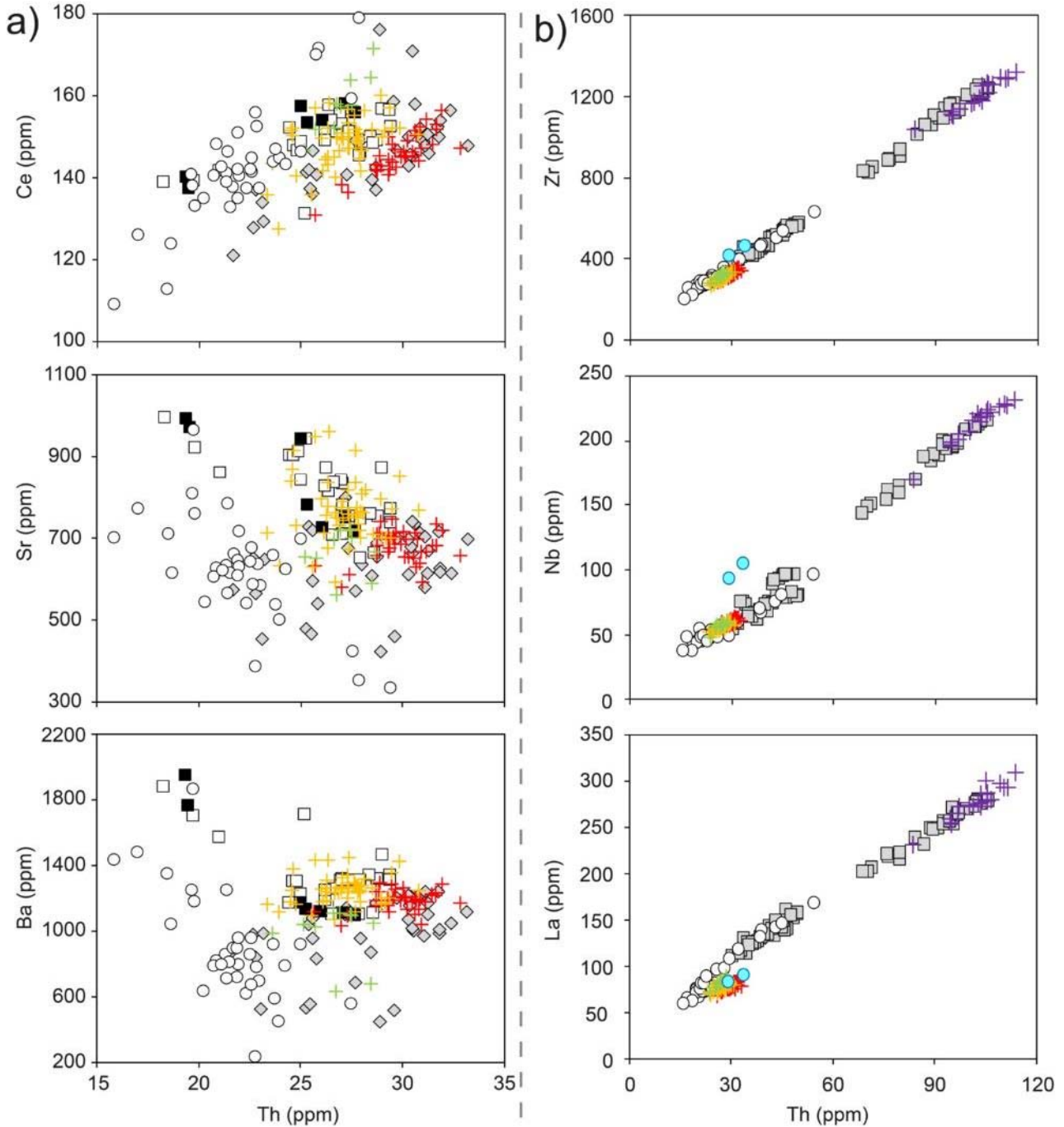
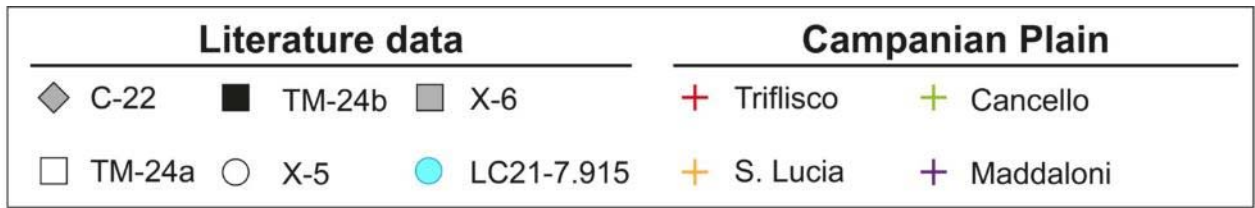
The POP1/TM-23-11/C-22 was also identified in Fucino succession, as layer TF-10 (Giaccio et al., 2017a), and in San Gregorio Magno basin, as layer S14, (Munno and Petrosino, 2007; Petrosino et al. 2019; Fig. 1a).

489 The C-22 was also correlated to the 11 cm- thick tephra layer CET1-10/14 in the Tyrrhenian core CET-1
490 (Petrosino et al., 2016). This marker was also identified in the marine core PRAD 1-2, in the Adriatic Sea, as
491 layer PRAD-2517 (Giaccio et al., 2012; Bourne et al., 2015). Finally, in the peatland succession of Tenaghi
492 Philippon, in Greece (Figs. 1a, 7), recent cryptotephra investigations by Wulf et al. (2018) allowed the
493 correlation of the C-22 marker with tephra layer TP05-25.195 (Fig. 5a).

494 **Santa Lucia** – Both major (Fig. 5b) and trace (Fig. 6a) element compositions, as well as the chronology of
495 Santa Lucia unit are compatible with TM-24a tephra of Monticchio, to which the Sulmona tephra POP2 was
496 also correlated (Giaccio et al., 2012; Fig. 7). The Monticchio varve-supported age for TM-24a is 102.0 ± 5.7
497 ka (Wulf et al, 2012; Monticchio chronology MON-2014, Sabine Wulf, personal communication 2017), whereas
498 the modelled age of POP2 is 102.0 ± 2.4 ka (Regattieri et al., 2015). In Sulmona paleo-hydrological record,
499 POP2 falls in the early stage of a period of increasing precipitation correlated to the Greenland Interstadial 23,
500 which in reference records (e.g., Corchia Cave, North Greenland Ice Core Project members et al., 2004;
501 Drysdale et al., 2007) starts about 102-103 ka, thus in agreement with the estimated age of POP2/TM-24a.
502 Here Santa Lucia unit is precisely $^{40}\text{Ar}/^{39}\text{Ar}$ dated at 101.2 ± 0.8 ka (Fig. 4b), supporting this correlation.
503 $^{87}\text{Sr}/^{86}\text{Sr}$ isotope ratios determined on Santa Lucia samples show values similar to those obtained for
504 Triflisco/C-22 tephra layer/marker (Fig. 3a), but they can be discriminated based on the higher HFSE (e.g., Th,
505 U) contents of the Triflisco/C-22 glasses than the Santa Lucia ones, thus preventing erroneous correlations
506 (Fig. 6a).

507 At Fucino Basin (Figs. 1a, 7), tephra layer TF-11, located immediately below tephra layer TF-10/C-22, was
508 correlated by Giaccio et al. (2017a) to the Monticchio tephra POP2/TM-24a (Fig. 7). The same marker horizon
509 was also recognized in Lake Ohrid (North Macedonia-Albania; Figs. 1a, 7) as layer OH-DP-0404 (Leicher et
510 al., 2016). The crypto-tephra CET1 12-13-14 in the Tyrrhenian core CET1 (Fig. 1a) also has major element
511 composition compatible with TM-24a/POP2 (Petrosino et al., 2016), thus representing the unique so far known
512 occurrence of Santa Lucia unit in the marine realm. Finally, at San Gregorio Magno (Munno and Petrosino,
513 2007; Petrosino et al., 2019), tephra layer S13, underlying tephra layer S14/C-22, would be stratigraphically
514 well suited to be a potential candidate for the TM-24a/Santa Lucia unit (Fig. 7). However, EDS-glass chemical
515 composition supports only partially this correlation (Fig. 5b), and WDS-glass composition should be acquired
516 on purpose.

517



518

519

520

521

522

523

524

525

Figure 6. Incompatible trace element patterns against Th for the Triflisco, Santa Lucia, Canello and Maddaloni units in comparison with literature data. Literature data source: C-22 = TM-23-11, PRAD 2525 (Bourne et al., 2015), S14 (Petrosino et al., 2019); TM-24a = TM-24a (Wulf et al., 2012); TM-24b = TM-24b (Wulf et al., 2012); X-5 = TM-25 (Wulf et al., 2012), POP-3 (Giaccio et al., 2012), LC21-7.915 (Satow et al., 2015), LeS1 (Donato et al., 2016), TF-12 (Giaccio et al., 2017a), S11 (Petrosino et al., 2019); X-6 = TM-27, PRAD 2812 (Bourne et al., 2015), LeS2 (Donato et al., 2016), TF-13 (Giaccio et al., 2017a), S10 (Petrosino et al., 2019).

Cancello – The Cancello pumice fall occurs below Santa Lucia unit=TM-24a/POP2 (Di Vito et al., 2008; Fig.

526

1b), thus indicating POP2a (Giaccio et al., 2012) and TM-24b (Wulf et al., 2012), which respectively underlay

527 POP2 and TM-24a, as the best candidates for correlation to this unit (Fig. 7). Major element biplots confirm
528 this correlation (Fig. 5c), also supported by trace element comparison (Fig. 6a). In particular, with respect to
529 the Santa Lucia unit, the Canello unit appears to extend to lower Th contents (Figs. 2f, 6a), which allows
530 discriminating these two tephra markers. At Monticchio, TM-24b is varve-dated at 103.1 ± 5.7 ka (Wulf et al.,
531 2012; MON-2014), while in Sulmona Basin a modelled age of 103.3 ± 1.4 ka was obtained for POP2a
532 (Regattieri et al., 2015), in agreement with the more precise age of 102.5 ± 0.8 ka here measured for the
533 Canello unit (Fig. 4c). In summary, the correlation of Canello unit to POP2a/TM-24b is fully supported by all
534 the geochemical and geochronological data.

535 At San Gregorio Magno (Munno and Petrosino, 2007; Petrosino et al., 2019), the tephra layer S12 is
536 stratigraphically well suited for being a good correlation candidate for POP2a/TM-24b (Fig. 7). The
537 geochemical correlation of S12 with Canello unit, based on the available EDS-glass composition, is quite
538 convincing (Fig. 5c), but more compelling WDS data would be required. Finally, the crypto-tephra CET1-15 in
539 the Tyrrhenian core CET1 (Fig. 1a) is stratigraphically (Fig. 7) and compositionally consistent with TM-
540 24b/POP2b (Petrosino et al., 2016).

541
542 **Maddaloni and Montemaoro** – At Masseria Montemaoro quarry (site Schiava - SC2; Fig. 1b and 1c), these
543 two, stratigraphically superimposed units underlie the Canello unit (Fig. 1c). The $^{40}\text{Ar}/^{39}\text{Ar}$ age of 109.3 ± 1.0
544 ka determined for Maddaloni unit is virtually indistinguishable from that of 109.1 ± 0.8 ka, obtained for the
545 Sulmona tephra layer POP4 (Regattieri et al., 2017), which was correlated to the X-6 tephra marker (Regattieri
546 et al., 2015), corresponding to the Monticchio TM-27 (Wulf et al., 2012). Consistent with this chronological
547 information, the major (Fig. 5d) and trace (Fig. 6b) elements composition of the Maddaloni unit well match the
548 most evolved term of POP4/TM-27 tephra layer/marker and those of the other X-6 equivalent layers in distal
549 archives through the central Mediterranean area (Fig. 1a). Sr-Nd isotope values obtained from the Maddaloni
550 unit are consistent with those of CIL-2/X-6 tephra layer/marker from the Cilento coast and other X-6
551 occurrences (Fig. 3a-b), thus further supporting its correlation with the X-6 marker. Moreover, major and trace
552 elements glass compositions are extremely distinctive (e.g., different alkali ratio and Cl content, incompatible
553 trace element patterns), and we thus highly recommend the employment of these geochemical tracers as a
554 correlation tool for the X-6 tephra (Figs. 5d, 6b; Supplementary Materials-1). All geochemical and chronological
555 data thus corroborate Maddaloni as the most proximal equivalent of the X-6 tephra marker.

556 The Ionian X-6 tephra marker (Keller et al., 1978), and its other marine and terrestrial equivalents, is the most
557 widespread MIS 5 Campi Flegrei tephra (Figs. 1a, 7), while considering the whole Campi Flegrei record, in

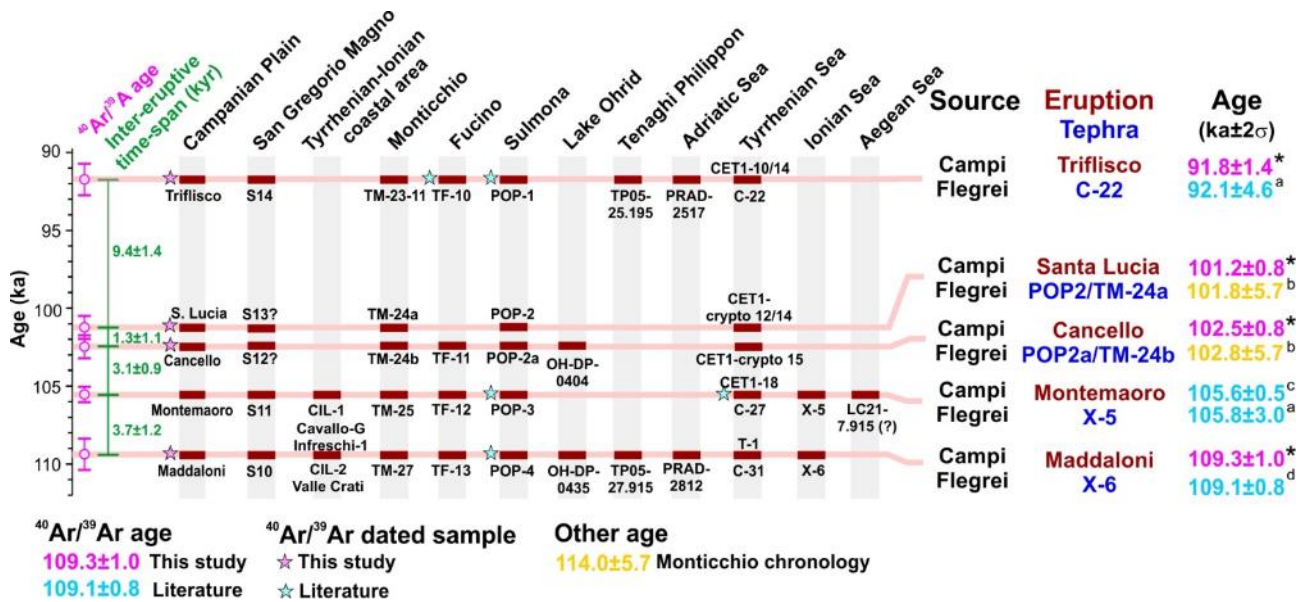
558 terms of dispersal area it is second only to the CI (e.g., [Costa et al., 2012](#)). It has been recognised in a series
559 of sedimentary successions in the central Mediterranean area ([Figs. 1a, 7](#)), including the Ionian Sea (I-9,
560 [Insinga et al., 2014](#)), Tyrrhenian Sea (C-31, [Paterne et al., 2008](#)), Adriatic Sea (PRAD-2812, [Bourne et al.](#)
561 [2015](#)), Fucino Basin (TF-13, [Giaccio et al., 2017a](#)), Cilento Coast ([Giaccio et al., 2012](#); [Donato et al., 2016](#)),
562 San Gregorio Magno Basin (S10, [Petrosino et al., 2019](#)), Valle del Crati (Tarsia, [Donato et al., 2016](#)), Grotta
563 del Cavallo Palaeolithic site (Unit G, [Zanchetta et al., 2018](#)), Lake Ohrid (OH-DP-0435, [Leicher et al., 2016](#)),
564 and Tenaghi Philippon (TP05-27.915, [Wulf et al., 2018](#)).

565 Regarding Montemaoro unit, its stratigraphic position between Maddaloni/X-6 and Canello/TM-24b, which
566 chronologically constrains it between ~109 ka and ~103 ka, makes it the best candidate for the terrestrial
567 counterpart of the Ionian Sea marker X-5, which lays immediately above the X-6 ([Keller et al., 1978](#)). The X-5
568 is equivalent to tephra layer TM-25 in the Lago Grande di Monticchio succession, dated at 105.6 ± 0.5 ka
569 (recalculated with ACs at 1.1891 Ma; Tyrrhenian Sea; [Petrosino et al., 2015](#)), or POP3 $^{40}\text{Ar}/^{39}\text{Ar}$ dated at 105.8
570 ± 1.3 ka (Sulmona Basin; [Giaccio et al., 2012](#)). Although it was not possible to acquire new major (glass-WDS)
571 and/or trace element data, the available glass-EDS composition for the Montemaoro unit supports this
572 correlation ([Fig. 5d](#)). Consequently, we suggest that the Montemaoro unit is the most likely proximal
573 counterpart of the X-5, based on the chronological and stratigraphical constraints provided in this study and
574 the existing chemical data. Future discovery of a new field exposure of Montemaoro would allow further
575 verification of this correlation.

576 Although less dispersed, the X-5 marker, like the X-6, was reported in several stratigraphic successions ([Figs.](#)
577 [1a, 7](#)), including the Fucino Basin (TF-12, [Giaccio et al., 2017a](#)), Cilento Coast (CIL1, [Giaccio et al., 2012](#);
578 LeS1, [Donato et al., 2016](#)), San Gregorio Magno Basin (S11, [Petrosino et al., 2019](#)), and as the lowermost
579 tephra layer in CET1 core (i.e., CET1-18, [Petrosino et al., 2015](#)), $^{40}\text{Ar}/^{39}\text{Ar}$ dated at 105.18 ± 0.5 ka (2σ
580 analytical uncertainty).

581 A potential correlative for either the X-6 or X-5 marker was also recognised at the remote site of marine core
582 LC21 ([Satow et al., 2015](#)), in the Aegean Sea ([Fig. 1a](#)). Specifically, the crypto-tephra LC21-7.915, whose
583 base was dated at 104.1 ± 2.2 ka, according to the LC21 age model ([Satow et al., 2015](#)), presents two
584 geochemical compositions indicating both Santorini and Campanian sources. The Campanian component is
585 in turn represented by two glass HAR and LAR trachyte-phonolite populations, which are compatible with X-5
586 and X-6 compositions, respectively ([Fig. 5d](#)). Moreover, in terms of trace element composition, the few
587 available data appear quite consistent with both markers ([Fig. 6b](#)). However, both the age and
588 climatostratigraphic position of the crypto-tephra LC21-7.915 make the X-5 the most probable correlative.

589 Indeed, LC21-7.915 precisely marks the onset of the sapropel S4 deposition, at the base of which in the
 590 Tyrrhenian Sea records the tephra X-5/C-27 is also found (Fig. 8; Pateme et al., 2008; Regattieri et al., 2015).
 591 Therefore, we are inclined to consider the X-5 as the most likely correlative for the HAR component of the
 592 Campanian portion of LC21-7.915 crypto-tephra, though the co-presence of the LAR component would require
 593 a plausible explanation.
 594 Overall, the correlations of the investigated Campanian Plain units with the five distal tephra markers are well
 595 supported by several lines of consistent, independent evidence, including their stratigraphic order,
 596 geochronology, and geochemistry (major and trace elements, and the Sr-Nd isotopes). However, in some
 597 cases, the geochemical variability of the investigated Campanian Plain units is less wide than the
 598 corresponding distal tephra. This is especially true for Canello and Maddaloni units, the composition of which
 599 covers only a part of the wider variability observed in distal settings (Figs. 5c-d, 6b). This is not surprising, as
 600 the occurrence of the analysed medial-distal units is relatively scant with respect to the distal ones, and thus
 601 could be not representative of the complete eruptive sequence and geochemical variability. This would suggest
 602 that not all the eruptive phases or sub-units, e.g., pyroclastic flow or fall, of Canello and Maddaloni units
 603 reached the distance of 30-40 km, at which the investigated sections are located (Fig. 1b) or had dispersal
 604 axes not compatible with pumice deposition in these localities.
 605



606
 607 **Figure 7.** Age and occurrences of the C-22, POP2/TM-24a, POP2a/TM-24b, X-5, and X-6 tephra markers in terrestrial and marine
 608 sedimentary environments through the Mediterranean region. ⁴⁰Ar/³⁹Ar ages are according to ACs at 1.1891 Ma and FCs at 28.294 Ma.
 609 * This study, ^a Giaccio et al. (2012); ^b Wulf et al. (2012); ^c Petrosino et al. (2016); ^d Regattieri et al. (2015).
 610

611 **5.3. Implications for the chronology of the millennial-scale climatic oscillations of the MIS 5c-d**

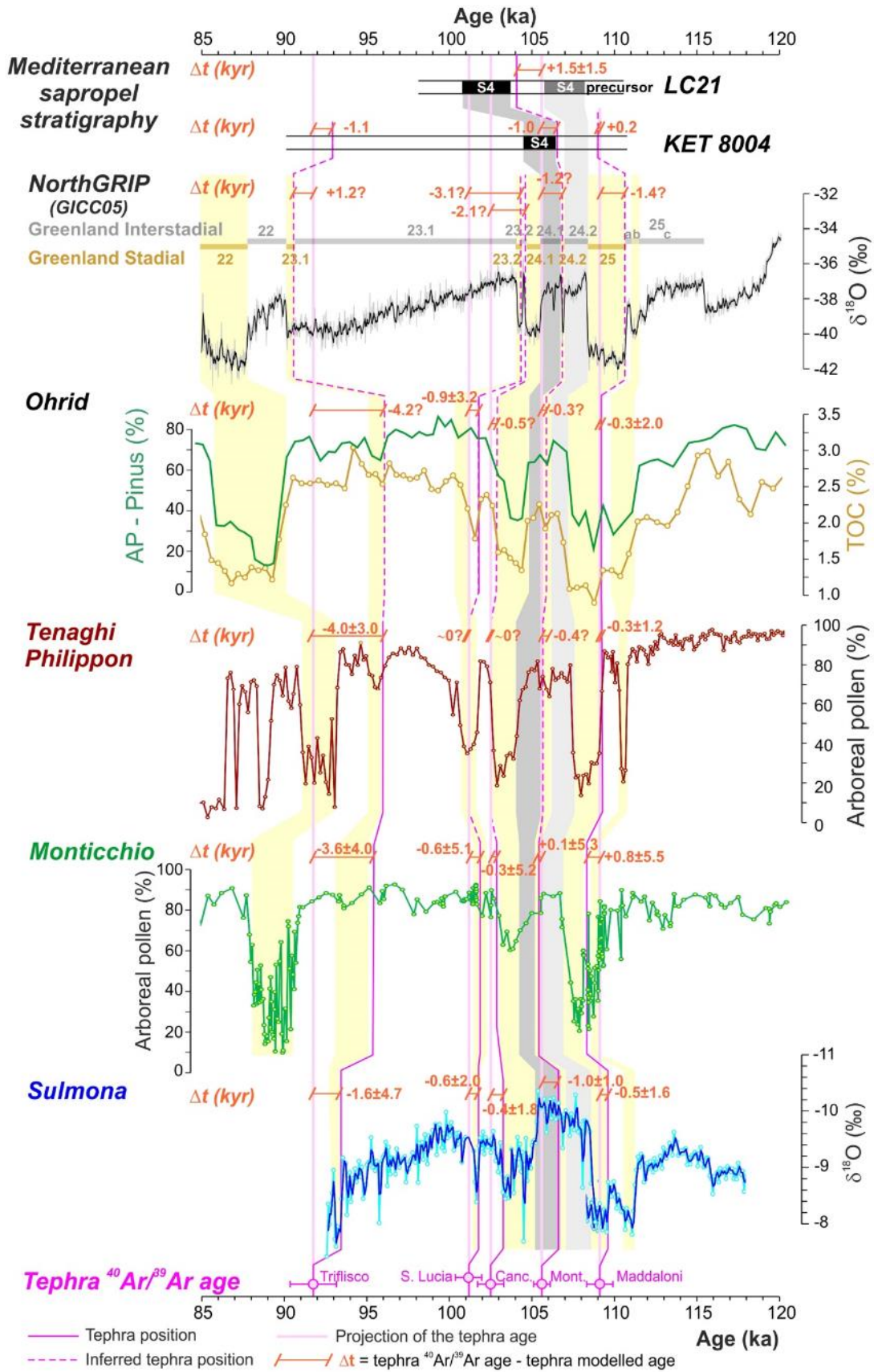
612 The great relevance of some of the investigated tephra layers as fundamental chronological and
 613 stratigraphic markers for the Mediterranean MIS 5c-d high frequency climatic variability was widely

614 acknowledged and discussed in previous papers (e.g., [Giaccio et al., 2012](#); [Regattieri et al., 2015](#)). However,
615 the acquisition of new high-precision $^{40}\text{Ar}/^{39}\text{Ar}$ ages for two previously undated tephra (Cancello/TM-24b and
616 Santa Lucia/TM-24a tephra layers/markers), the substantial improvement in accuracy of the Triflisco/C-22 unit,
617 as well as the acquisition of new high-resolution records containing these tephra markers (e.g., Tenaghi
618 Philippon; [Wulf et al., 2018](#)), give us the opportunity to discuss the implications of these new data from a
619 palaeoclimatological perspective, in particular on the timing and spatial synchronicity of MIS 5c-d climatic
620 variability.

621 For this purpose, we consider the records endowed with suitable resolution and good expression of the
622 millennial scale climate oscillations of the MIS 5d-c, which can be reasonably correlated to the succession of
623 stadial and interstadial events documented in the reference record of the Greenland ice (e.g., [North Greenland
624 Ice Core Project members et al., 2004](#)). These are (i) the Lago Grande di Monticchio pollen profile, Southern
625 Italy (e.g., [Brauer et al., 2007](#); [Wulf et al., 2012](#)), (ii) the isotope series of Sulmona Basin, Central Italy
626 ([Regattieri et al., 2015, 2017](#)), (iii) the Tenaghi Philippon pollen record, in Greece ([Milner et al., 2012, 2013,
627 2016](#)), and (iv) the pollen record of Lake Ohrid, North Macedonia-Albania ([Sinopoli et al., 2018](#); [Figs. 1a, 8](#)).
628 For the sapropel stratigraphy, we also consider the Tyrrhenian Sea record of the core KET 8004 ([Paterne et
629 al., 2008](#)), which contains three out of the five markers ([Fig. 8](#)), and the Aegean Sea core LC21, likely
630 containing the X-5 layer ([Satow et al., 2015](#); [Fig. 8](#)).

631 So far, Monticchio and Sulmona are the only Mediterranean records containing all the five MIS 5d-c tephra
632 from Campi Flegrei ([Fig. 8](#)), whereas Tenaghi Philippon and Ohrid contain only two markers, i.e., Maddaloni/X-
633 6 and Triflisco/C-22, and Maddaloni/X-6 and Santa Lucia/TM-24a, respectively ([Fig. 8](#); [Table 3](#)).

634 The Maddaloni/X-6 unit, the most common tephra in the considered records ([Fig. 7](#)), occurs at the very end of
635 a short interstadial pulsation, likely corresponding to Greenland Interstadial (GI) 25a. It precedes the onset of
636 the first marked stadial oscillation of the MIS 5 period, the Greenland Stadial (GS) 25a, corresponding to the
637 North Atlantic cold event C24 (e.g., [Shackleton et al., 2004](#); [Fig. 8](#)). The temporal offset, i.e., the difference
638 between the radioisotopic $^{40}\text{Ar}/^{39}\text{Ar}$ age of Maddaloni/X-6 tephra and the age reported in the various
639 paleoclimatic records (Δt in [Fig. 8](#)), is small, reaching the maximum value of ca. 1 kyr in the Monticchio record
640 ([Fig. 8](#); [Table 3](#)). However, assuming that the inferred position of Maddaloni/X-6 tephra layer/marker in the
641 Greenland isotope record is correct, then, the age of the end of the GI-25a, 110.6 ka, according to GICC05
642 ([Rasmussen et al., 2014](#)), should be approximately 1.3 kyr younger ([Fig. 8](#)). On the contrary, Sardinian
643 stalagmite evidence suggests instead that the GI-25b ended at 110.5 ka ([Columbu et al., 2017](#)), which is fully
644 consistent with the GICC05 chronology.



645
646
647
648
649
650
651
652

Figure 8. Chronological offset between $^{40}\text{Ar}/^{39}\text{Ar}$ and modelled tephra age in selected high-resolution Mediterranean records containing the here investigated tephra and showing the millennial-scale climatic oscillations of the MIS 5d-c, compared to Greenland ice succession of stadal-interstadial events (Rasmussen et al., 2014). The Mediterranean sapropel stratigraphy from the Tyrrhenian Sea core KET 8004 (Paterne et al., 2008) and Aegean Sea core LC21 (Satow et al., 2015), is also shown. The sapropel nomenclature is according to Ziegler et al. (2010). Data source: Lake Ohrid Arboreal pollen minus *Pinus* (AP – Pinus) and total organic carbon (TOC): Sinopoli et al. (2018), Wagner et al. (2017, 2019); Tenaghi Philippon pollen record: Milner et al. (2012, 2013, 2016); Monticchio pollen record: Brauer et al. (2007); Sulmona isotope record: Regattieri et al (2015).

653 The Montemaoro/X-5 tephra occurs in the middle of an interstadial oscillation correlated to the GI-24 (e.g.,
654 [Regattieri et al., 2015](#)). More precisely, Montemaoro/X-5 tephra occurs close to a very brief stadial pulsation
655 within the GI-24 that is quite evident in all the considered records and that likely corresponds to the short GS-
656 24.2 ([Fig. 8](#)). The Δt , relative to the Montemaoro/X-5 tephra, is of ca. 1 kyr in all records, except Monticchio, in
657 which it is negligible ([Fig. 8](#); [Table 3](#)). In the Tyrrhenian Sea, and likely in the Aegean Sea, the Montemaoro/X-
658 5 also represents an excellent marker for the Sapropel S4, which is in turn correlated to the GI-24.1 ([Regattieri](#)
659 [et al., 2015](#); [Fig. 8](#)).

660 The Canello and Santa Lucia tephra layers form an interesting couplet of temporally closely related tephra,
661 which mark the onset of an interstadial and the ensuing stadial phase, likely corresponding to the GI-23.2 and
662 the GS-23.2, respectively ([Fig. 8](#)). In all the considered records, the negligible Δt relative to this couple of
663 tephra evidences a good agreement between the $^{40}\text{Ar}/^{39}\text{Ar}$ chronology and the age models of the records ([Fig.](#)
664 [8](#)).

665 Finally, the Triflisco/C-22 tephra occurs at the beginning of a stadial event that interrupts a relatively long
666 interstadial period, likely corresponding to the GS-23.1, which occurs at the end of the long-term cooling period
667 featuring the GI-23.1 ([Fig. 8](#)). Noteworthy, the Δt relative to this tephra is quite long for the Monticchio and
668 Tenaghi Philippon pollen records, reaching the considerable value of ca. 4 kyr ([Fig. 8](#)). The Δt is instead quite
669 negligible for the NorthGRIP record (~1.2 kyr), provided that the inferred climatostratigraphic position of
670 Triflisco/C-22 in the Greenland record is correct.

671 **Table 3.** Detailed climatostratigraphic position of the Campi Flegrei units with respect to the millennial to sub-millennial scale MIS 5
672 paleoclimatic events - expressed as Greenland stadial-interstadial successions ([Rasmussen et al., 2014](#)) - as recorded in reference
673 archives of the central Mediterranean area ([Figs. 1, 7 and 8](#)). The temporal offset, i.e., the difference between the radioisotopic $^{40}\text{Ar}/^{39}\text{Ar}$
674 age of Campi Flegrei tephra and the age of the corresponding distal tephra, as reported in the various paleoclimatic records, is also
675 shown. Data source: Sulmona: [Regattieri et al. \(2015, 2017\)](#); Monticchio: [Wulf et al. \(2012\)](#), [Regattieri et al. \(2015\)](#); Ohrid: [Leicher et al.](#)
676 [\(2021\)](#); Tenaghi-Philippon: [Wulf et al. \(2018\)](#); LC21: [Satow et al. \(2015\)](#).

Campanian Plain	Sulmona	Monticchio	Ohrid	Tenaghi-Philippon	LC21	Correlated event
Tephra $^{40}\text{Ar}/^{39}\text{Ar}$ age (ka \pm 2 σ)	Tephra Age \pm 2 σ ka $\Delta t\pm$ 2 σ kyr	Tephra Age \pm 2 σ ka $\Delta t\pm$ 2 σ kyr	Tephra Age \pm 2 σ ka $\Delta t\pm$ 2 σ kyr	Tephra Age \pm 2 σ ka $\Delta t\pm$ 2 σ kyr	Tephra Age \pm 2 σ ka $\Delta t\pm$ 2 σ kyr	
Triflisco 91.8 \pm 1.4	POP1 93.4 \pm 4.5 -1.6 \pm 4.7	TM-23-11 95.4 \pm 3.8 -3.6 \pm 4.0		TP05-25.195 95.8 \pm 2.6 -4.0 \pm 3.0		Onset GS-23.1
Santa Lucia 101.2 \pm 0.8	POP2 101.8 \pm 1.8 -0.6 \pm 2.0	TM-24a 101.8 \pm 5.0 -0.6 \pm 5.1	OH-DP-0404 102.1 \pm 3.1 -0.9 \pm 3.2			Middle GS-23.2
Canello 102.5 \pm 0.8	POP2a 102.9 \pm 1.5 -0.4 \pm 1.7	TM-24b 102.8 \pm 5.1 -0.3 \pm 5.2				Onset GI-23.2
Montemaoro 105.6 \pm 0.5	POP3 106.6 \pm 1.0 -1.0 \pm 1.0	TM-25 105.5 \pm 5.3 0.1 \pm 5.3			LC21-7.915 (?) 104.0 \pm 2.0 1.5 \pm 1.5	End GS-24.2 - base sapropel S4
Maddaloni 109.1 \pm 0.8	POP4 109.6 \pm 1.4 -0.5 \pm 1.6	TM-27 108.3 \pm 5.4 0.8 \pm 5.5	OH-DP-0435 109.4 \pm 1.8 -0.3 \pm 2.0	TP05-27.915 109.4 \pm 0.9 -0.3 \pm 1.2		Onset GS-25 - End GI-25a

677

678 In summary, the Δt is relatively little for most of the climatic events, for which the Campi Flegrei MIS 5 tephra
679 act as fundamental markers, and generally do not exceed the uncertainty associated to both $^{40}\text{Ar}/^{39}\text{Ar}$ ages
680 and the age models of the respective paleoclimatic records (Table 3). However, the event associated with the
681 Triflisco/C-22 represents a notable exception, for which the Δt can exceed the uncertainty associated to the
682 $^{40}\text{Ar}/^{39}\text{Ar}$ dating of Triflisco/C-22 and of the paleoclimatic record age models (Figs. 7, 8; Table 3). With this
683 regard, we emphasize that such wide Δt cannot be explained invoking an uncertainty of the tephra position
684 within the records, as, at least for Monticchio and Tenaghi Philippon, where the Δt is -3.6 ± 4.0 kyr and $-4.0 \pm$
685 3.0 kyr (Table 3), it is not relayed on an inference, this being based on undisputable stratigraphic evidence
686 (Fig. 8).

687 Overall, the investigated tephra can be considered good stratigraphic markers of some of the stadial-
688 interstadial events, as well as of the very short sub-stadial and sub-interstadial oscillations that punctuated the
689 MIS 5c-d climatic variability (Table 3), whose chronology can greatly benefit from the high precision $^{40}\text{Ar}/^{39}\text{Ar}$
690 dating of the Campi Flegrei eruption products.

691

692

693 6. Conclusions

694 In this study, we presented a wide dataset (i.e., stratigraphy, major, minor, and trace elements, Sr-Nd
695 isotopic composition and $^{40}\text{Ar}/^{39}\text{Ar}$ ages) required for a full characterization of four pumice fall deposits, named
696 Triflisco, Santa Lucia, Cancellò, and Maddaloni, occurring in the Campanian Plain, 30 to 60 km east of the
697 Campi Flegrei volcanic field, and stratigraphically laying below the CI (~40 ka). Based on these data, these
698 units are here attributed to a previously unknown 109-92 ka explosive activity at Campi Flegrei volcano and
699 correlated with the widespread C-22, TM-24a/POP-2, TM-24b/POP-2a and X-6 tephra markers, respectively.
700 Furthermore, the chronological and stratigraphic constraints provided in this study, and a review of previous
701 EDS data, allow us also to propose the correlation of a fifth unit (i.e., Montemaoro) with the X-5 marine tephra
702 marker as well.

703 Our data confidently allow us to trace the volcanic source of these fundamental Mediterranean marker
704 horizons, so far only hypothesized. This extends the activity history of the Campi Flegrei volcano back ~110
705 ka at least, setting the groundwork for a reassessment of the volcanic history, and related hazards, and
706 confirming the Campi Flegrei volcano as one of the Europe's most productive sources of widespread and
707 disruptive ash fall events. The Maddaloni/X-6, given its wide dispersal area, clearly arises from one of the

708 largest explosive events through the whole Campi Flegrei eruptive history and demands further volcanological
709 investigations.

710 The new high-precision $^{40}\text{Ar}/^{39}\text{Ar}$ dating of the investigated units provide new fundamental temporal constraints
711 for refining and consolidating the chronology of MIS 5d-c period, characterised by a marked millennial- to sub-
712 millennial scale climatic variability, well documented in Mediterranean archives. Specifically, the ages obtained
713 for the Canello and Santa Lucia tephra markers provide two new chronological constraints for the climatic
714 oscillations likely corresponding to the Greenland interstadial GI-23.2 and Greenland stadial GS-23.2.
715 Furthermore, the improved precision of the age for Triflisco would imply a substantial extension of the duration
716 of the interstadial period corresponding to the GI-23.1 up to 92 ka, i.e., ~4 kyr later than the ~96 ka age reported
717 for the GI-23.1 in several reference Mediterranean records. (Fig. 8). A reappraisal of the related chronologies
718 is thus required.

719 Future research development on the eruptive history and long-term hazard assessment at Campi Flegrei, as
720 well as paleoclimatic and archaeological investigations in central Mediterranean, will greatly benefit from the
721 geochemical and geochronological dataset provided in this contribution. Given the strong geochemical
722 similarities of the HAR Triflisco/C-22, Santa Lucia/TM-24a, and Canello/TM-24b units, we encourage caution
723 to avoid potentially misleading correlations based solely on major elements. Therefore, especially when a
724 specific tephra layer occurrence lacks bracketing tephra units, we recommend integrating major element data
725 with trace element and Sr-Nd isotope analysis, as they proved to be the best discriminating tool for these
726 tephra deposits.

727 728 **Acknowledgments**

729 R. Jedlička and M. Racek, E. Braschi and A. Orlando, are thanked for providing valuable technical assistance during EPMA analysis at
730 Prague and Florence Universities respectively. Field activities of L.M. were financially supported by "Sapienza" University, "Bando di Avvio
731 alla Ricerca", protocol N° AR120172AD35B81D (responsible: L.M.). G.S. received funding by "Sapienza" University, Fondi di Ateneo-
732 Progetti Medi (protocol N° RM11715C82384428). Financial support was provided by the Competitive fund of the Italian Research Ministry
733 (MUR, PRIN 2017, grant 20177TKBXZ_003, project "FUTURE, G. Zanchetta, coordinator), issued to BG, DP and GZ. The INGV-OV
734 laboratories have been also financially supported by the EPOS Research Infrastructure through the contribution of the Italian Ministry of
735 University and Research (MUR). P.G.A. is funded through a UK Research and Innovation (UKRI) Future Leaders Fellowship
736 (MR/S035478/1). An earlier version of the manuscript benefited from useful comments from R. Cioni and Sabine Wulf. Ioan Seghedi (IG
737 "SSS" AR) and an anonymous reviewer provided thoughtful and constructive comments that improved the manuscript.
738

739
740
741
742
743
744
745
746
747
748
749
750
751
752
753
754
755
756
757
758
759
760
761
762
763
764
765
766
767
768
769
770
771
772
773
774
775
776
777
778
779
780
781
782
783
784
785
786
787
788
789
790
791
792
793
794
795
796
797
798
799
800
801
802
803
804

References

- Albert, P.G., Giaccio, B., Isaia, R., Costa, A., Niespolo, E.M., Nomade, S., Pereira, A., Renne, P.R., Hinchliffe, A., Mark, D.F., Brown, R.J., Smith, V.C., 2019. Evidence for a large-magnitude eruption from Campi Flegrei Caldera (Italy) at 29 ka. *Geology* **47** (7), 595-599. <https://doi.org/10.1130/G45805.1>.
- Albert, P.G., Hardiman, M., Keller, J., Tomlinson, E.L., Smith, V.C., Bourne, A.J., Wulf, S., Zanchetta, G., Sulpizio, R., Müller, U.C., Pross, J., Ottolini, L., Matthews, I.P., Blockley, S.P.E., Menzies, M.A., 2015. Revisiting the Y-3 stratigraphic marker: a new diagnostic glass geochemistry, age estimate, and details on its climatostratigraphical context. *Quat. Sci. Rev.* **118**, 105-121. <https://doi.org/10.1016/j.quascirev.2014.04.002>.
- Andronico, D. & Cioni, R., 2002. Contrasting styles of Mount Vesuvius activity in the period between the Avellino and Pompeii Plinian eruptions, and some implications for assessment of future hazards. *Bull. Volcanol.* **64**, 372-391. <https://doi.org/10.1007/s00445-002-0215-4>.
- Arienzo, I., Civetta, L., Heumann, A., Wörner, G., Orsi, G., 2009. Isotopic evidence for open system processes within the Campanian Ignimbrite (Campi Flegrei-Italy) magma chamber. *Bull. Volcanol.* **71**, 285-300. <https://doi.org/10.1007/s00445-008-0223-0>.
- Arienzo, I., D'Antonio, M., Di Renzo, V., Tonarini, S., Minolfi, G., Orsi, G., Carandente, A., Belviso, P., Civetta, L., 2015. Isotopic microanalysis sheds light on the magmatic endmembers feeding volcanic eruptions: The Astroni 6 case study (Campi Flegrei, Italy). *J. Volcanol. Geotherm. Res.* **304**, 24-37. <https://doi.org/10.1016/j.jvolgeores.2015.08.003>.
- Arienzo, I., Mazzeo, F.C., Moretti, R., Cavallo, A., D'Antonio, M., 2016. Open-system magma evolution and fluid transfer at Campi Flegrei caldera (Southern Italy) during the past 5 ka as revealed by geochemical and isotopic data: the archetype of Nisida eruption. *Chem. Geol.* **427**, 109-124. <https://doi.org/10.1016/j.chemgeo.2016.02.007>.
- Arienzo, I., Moretti, R., Civetta, L., Orsi, G., Papale, P., 2010. The feeding system of the Agnano-Monte Spina eruption Campi Flegrei, Italy): dragging the past into present activity and future scenarios. *Chem. Geol.* **270** (1-4), 135-147. <https://doi.org/10.1016/j.chemgeo.2009.11.012>.
- Balbas, A., Koppers, A.A.P., Kent, D.V., Konrad, K., Clark, P.U., 2016. Identification of the short-lived Santa Rosa geomagnetic excursion in lavas on Floreana Island (Galapagos) by ⁴⁰Ar/³⁹Ar geochronology. *Geology* **44** (5), 359-362 (2016). <https://doi.org/10.1130/G37569.1>.
- Bourne, A.J., Albert, P.G., Matthews, I.P., Trincardi, F., Wulf, S., Asioli, A., Blockley, S.P.E., Keller, J., Lowe, J.J., 2015. Tephrochronology of core PRAD 1-2 from the Adriatic Sea: insights into Italian explosive volcanism for the period 200-80 ka. *Quat. Sci. Rev.* **116**, 28-43. <https://doi.org/10.1016/j.quascirev.2015.03.006>.
- Bourne, A.J., Lowe, J.J., Trincardi, F., Asioli, A., Blockley, S.P.E., Wulf, S., Matthews, I.P., Piva, A., Vigliotti, L., 2010. Distal tephra record for the last ca 105,000 years from core PRAD 1-2 in the central Adriatic Sea: implications for the marine tephrostratigraphy. *Quat. Sci. Rev.* **29**, 3079-3094. <https://doi.org/10.1016/j.quascirev.2010.07.021>.
- Brauer, A., Allen, J.R.M., Mingram, J., Dulski, P., Wulf, S., Huntley, B., 2007. Evidence for the last interglacial chronology and environmental change from Southern Europe. *PNAS* **104** (2), 450-455. <https://doi.org/10.1073/pnas.0603321104>.
- Brown, R.J., Civetta, L., Arienzo, I., D'Antonio, M., Moretti, R., Orsi, G., Tomlinson, E.L., Albert, P.G., Menzies, M.A., 2014. Geochemical and isotopic insights into the assembly, evolution and disruption of a magmatic plumbing system before and after cataclysmic caldera-collapse eruption at Ischia volcano (Italy). *Contrib. Mineral. Petrol.* **168**: 1035. <https://doi.org/10.1007/s00410-014-1035-1>.
- Brown, R.J., Orsi, G., de Vita, S., 2008. New insights into Late Pleistocene explosive volcanic activity and caldera formation on Ischia. *Bull. Volcanol.* **70**, 583-603. <https://doi.org/10.1007/s00445-007-0155-0>.
- Casalini, M., Heumann, A., Marchionni, S., Conticelli, S., Avanzinelli, R., Tommasini, S., 2018. Inverse modelling to unravel the radiogenic isotope signature of mantle sources from evolved magmas: the case-study of Ischia volcano. *Ital. J. Geosci.* **137**, pp. 00. <https://doi.org/10.1033011JG.2018.05>.
- Civetta, L., Orsi, G., Pappalardo, L., Fisher, R.V., Heiken, G., Ort, M., 1997. Geochemical zoning, mingling, eruptive dynamics and depositional processes - the Campanian Ignimbrite, Campi Flegrei, Italy. *J. Volcanol. Geotherm. Res.* **75** (3-4), 183-219. [https://doi.org/10.1016/S0377-0273\(96\)00027-3](https://doi.org/10.1016/S0377-0273(96)00027-3).
- Columbu, A., Drysdale, R., Capron, E., Woodhead, J., De Waele, J., Sanna, L., Hellstrom, J., Bajo, P., 2017. Early last glacial intra-interstadial climate variability recorded in Sardinian speleothem. *Quat. Sci. Rev.* **169**, 391-397. <https://doi.org/10.1016/j.quascirev.2017.05.007>.
- Costa, A., Folch, A., Macedonio, G., Giaccio, B., Isaia, R., Smith, V.R., 2012. Quantifying volcanic ash dispersal and impact of the Campanian Ignimbrite super-eruption. *Geophys. Res. Lett.* **39**, p. L101310. <https://doi.org/10.1029/2012GL051605>.
- Cox, S.E., Hemming, S.R., Tootell, D., 2020 The Isotopx NGX and ATONA Faraday amplifiers. *Geochronology* **2**, 231-243. <https://doi.org/10.5194/gchron-2-231-2020>.
- D'Antonio, M., Arienzo, I., Brown, R.J., Petrosino, P., Pelullo, C., Giaccio, B., 2021. Petrography and mineral chemistry of Monte Epomeo Green Tuff, Ischia Island, South Italy: Constraints for identification of the Y-7 tephrostratigraphic marker in distal sequences of the Central Mediterranean. *Minerals* **11**, 955. <https://doi.org/10.3390/min11090955>.
- D'Antonio, M., Tonarini, S., Arienzo, I., Civetta, L., Dallai, L., Moretti, R., Orsi, G., Andria, M., Trecalli, A., 2013. Mantle and crustal processes in the magmatism of the Campania region: inferences from mineralogy, geochemistry, and Sr-Nd-O isotopes of young hybrid volcanics of the Ischia island (South Italy). *Contrib. Mineral. Petrol.* **165**, 1173-1194. <https://doi.org/10.1007/s00410-013-0853-x>.
- D'Antonio, M., Tonarini, S., Arienzo, I., Civetta, L., Di Renzo, V., 2007. Components and processes in the magma genesis of the Phlegrean Volcanic District, southern Italy. In: Beccaluva, L., Bianchini, G., Wilson, M. (eds.) *Cenozoic Volcanism in the Mediterranean Area. Geol. Soc. Am. Special Paper* **418**, 203-220.
- De Astis, G., Pappalardo, L., Piochi, M., 2004. Procida volcanic history: new insights into the evolution of the Phlegrean Volcanic District (Campania region, Italy). *Bull. Volcanol.* **66**, 622-641. <https://doi.org/10.1007/s00445-004-0345-y>.
- De Vivo, B., Rolandi, G., Gans, P.B., Calvert, A., Bohrsen, W.A., Spera, F.J., Belkin, H.E., 2001. New constraints on the pyroclastic eruptive history of Campanian volcanic Plain (Italy). *Mineral. Petrol.* **73**, 47-65. <https://doi.org/10.1007/s007100170010>.

- 805 Deino, A.L., Orsi, G., de Vita, S., Piochi, M., 2004. The age of the Neapolitan Yellow Tuff caldera-forming eruption (Campi Flegrei Caldera
806 - Italy) assessed by $^{40}\text{Ar}/^{39}\text{Ar}$ dating method. *J. Volcanol. Geotherm. Res.* **133** (1-4), 157-170. [https://doi.org/10.1016/S0377-0273\(03\)00396-2](https://doi.org/10.1016/S0377-0273(03)00396-2).
- 807
- 808 Di Renzo, V., Arienzo, I., Civetta, L., D'Antonio, M., Tonarini, S., Di Vito, M.A., Orsi, G., 2011. The magmatic feeding system of the Campi
809 Flegrei caldera: Architecture and temporal evolution. *Chem. Geol.* **281** (3-4), 227-241. <https://doi.org/10.1016/j.chemgeo.2010.12.010>.
- 810 Di Vito, M.A., Sulpizio, R., Zanchetta, G., D'Orazio M., 2008 The late Pleistocene pyroclastic deposits of the Campanian Plain: New
811 insights into the explosive activity of the Neapolitan volcanoes. *J. Volcanol. Geotherm. Res.* **177**, 19-48.
812 <https://doi.org/10.1016/j.jvolgeores.2007.11.019>.
- 813 Donato, P., Albert, P.G., Crocitti, M., De Rosa, C., Menzies, M.A., 2016. Tephra layers along the southern Tyrrhenian coast of Italy: Links
814 to the X-5 & X-6 using volcanic glass geochemistry. *J. Volcanol. Geotherm. Res.* **317**, 30-41.
815 <https://doi.org/10.1016/j.jvolgeores.2016.02.023>.
- 816 Drysdale, R., Zanchetta, G., Hellstrom, J.C., Fallick, A.E., McDonald, J., Catwright, I., 2007. Stalagmite evidence for the precise timing of
817 North Atlantic cold events during the early last glacial. *Geology* **35** (1), 77-80. <https://doi.org/10.1130/G23161A.1>.
- 818 Fanara, S., Botcharnikov, R.E., Palladino, D.M., Adams, F., Buddensieck, J., Mulch, A., Behrens, H., 2015. Volatiles in magma related to
819 Campanian Ignimbrite eruption: Experiments vs natural findings. *Am. Min.* **100** (10), 2284-2297. <https://doi.org/10.2138/am-2015-5033>.
- 820
- 821 Galli, P., Giaccio, B., Messina, P., Peronace, E., Amato, V., Naso, G., Nomade, S., Pereira, A., Piscitelli, S., Bellanova, J., Billi, A., Blamart,
822 D., Galderisi, A., Giocoli, A., Stabile, T., Thil, F., 2017. Middle to Late Pleistocene activity of the Matese fault system (southern
823 Apennines, Italy). *Tectonophysics* **699**, 61-81. <https://doi.org/10.1016/j.tecto.2017.01.007>.
- 824 Giaccio, B., Haydas, I., Isaia, R., Deino, A., Nomade, S., 2017b. High-precision ^{14}C and $^{40}\text{Ar}/^{39}\text{Ar}$ dating of Campanian Ignimbrite (Y-5)
825 reconciles the time-scales of climatic cultural processes at 40 ka. *Sci. Rep.* **7**, 45940. <https://doi.org/10.1038/srep45940>.
- 826 Giaccio, B., Niespolo, E.M., Pereira, A., Nomade, S., Renne, P.R., Albert, P.G., Arienzo, I., Regattieri, E., Wagner, B., Zanchetta, G.,
827 Gaeta, M., Galli, P., Mannella, G., Peronace, E., Sottili, G., Florindo, F., Leicher, N., Marra, F., Tomlinson, E.L., 2017a. First integrated
828 tephrochronological record for the last ~190 kyr from the Fucino Quaternary lacustrine succession, central Italy. *Quat. Sci. Rev.* **158**,
829 211-234. <https://doi.org/10.1016/j.quascirev.2017.01.004>.
- 830 Giaccio, B., Nomade, S., Wulf, S., Isaia, R., Sottili, G., Cavuoto, G., Galli, P., Messina, P., Sposato, A., Sulpizio, R., Zanchetta, G., 2012.
831 The late MIS 5 Mediterranean tephra markers: a reappraisal from peninsular Italy terrestrial records. *Quat. Sci. Rev.* **56**, 31-45.
832 <https://doi.org/10.1016/j.quascirev.2012.09.009>.
- 833 Goldstein, S.L., Denis, P., Oelkers, E.H., Rudnick, R.L., Walter, L.M., 2003. Standards for publication of isotope ratio and chemical data
834 in chemical geology. *Chem. Geol.* **202**, 1-4. <https://doi.org/10.1016/j.chemgeo.2003.08.003>.
- 835 Insinga, D.D., Tamburrino, S., Lirer, F., Vezzoli, L., Barra, M., De Lange, G.J., Tiepolo, M., Vallefucio, M., Mazzola, S., Sprovieri, M.,
836 2014. Tephrochronology of the astronomically-tuned KC01B deep-sea core, Ionian Sea: insights into the explosive activity of the
837 Central Mediterranean area during the last 200 ka. *Quat. Sci. Rev.* **85**, 63-84. <https://doi.org/10.1016/j.quascirev.2013.11.019>.
- 838 Iorio, M., Liddicoat, J., Budillon, F., Incoronato, A., Coe, R.S., Insinga, D.D., Cassata, W.S., Lubritto, C., Angelino, A., Tamburrino, S.,
839 2014. Combined palaeomagnetic secular variation and petrophysical records to time-constrain geological and hazardous events: An
840 example from the eastern Tyrrhenian Sea over the last 120 ka. *Glob. Planet Change* **113**, 91-109.
841 <https://doi.org/10.1016/j.gloplacha.2013.11.005>.
- 842 Jochum, K.P., Stoll, B., Herwig, K., Willbold, M., Hofmann, A.W., Amini, M., Aarbug, S., Abouchami, W., Hellebrand, E., Mocek, B.,
843 Raczek, I., Stracke, A., Alard, O., Bouman, C., Becker, S., Dücking, M., Brätz, H., Klemd, R., de Bruin, D., Canil, D., Cornell, D., de
844 Hoog, C.-S., Dalpé, C., Danyushevsky, L., Eisenhauer, A., Gao, Y., Snow, J.E., Groschopf, N., Günther, D., Latkoczy, C., Guillong,
845 M., Hauri, E.K., Höfer, H.E., Lahaye, Y., Horz, K., Jacob, D.E., Kasemann, S.A., Kent, A.J.R., Ludwig, T., Zack, T., Mason, P.R.D.,
846 Meixner, A., Rosner, M., Kisawa, K., Nash, P.B., Pfänder, J., Premo, W.R., Sun, W.D., Tiepolo, M., Vannucci, R., Vennemann, T.,
847 Wayne, D., Woodhead, J.D., 2006. MPI-DING reference glasses for in situ microanalysis: New reference values for element
848 concentrations and isotope ratios. *Geochem. Geophys.* **7**:2. <https://doi.org/10.1029/2005GC001060>.
- 849 Keller, J., Ryan, W.B.F., Ninkovich, D., Altherr, R., 1978. Explosive volcanic activity in the Mediterranean over the last 200,000 yr as
850 recorded in deep-sea sediments. *Geol. Soc. Am. Bull.* **89**, 591-604. [https://doi.org/10.1130/0016-7606\(1978\)89%3C591:EVAITM%3E2.0.CO;2](https://doi.org/10.1130/0016-7606(1978)89%3C591:EVAITM%3E2.0.CO;2).
- 851 Koppers, A.A.P., 2002. ArArCALC e software for $^{40}\text{Ar}/^{39}\text{Ar}$ age calculations. *Comput. Geosci.* **28**, 605-619. [https://doi.org/10.1016/S0098-3004\(01\)00095-4](https://doi.org/10.1016/S0098-3004(01)00095-4).
- 852
- 853 Kuehn, S.C., Froese, D.G., Shane, P.A.R., INTAV Intercomparison Participants, 2011. The INTAV intercomparison of electron-beam
854 microanalysis of glass by tephrochronology laboratories: Results and recommendations. *Quat. Int.* **246** (1-2), 19-47.
855 <https://doi.org/10.1016/j.quaint.2011.08.022>.
- 856
- 857 Le Maitre, R.W., Streckeisen, A., Zanettin, B., Le Bas, M.J., Bonin, B., Bateman, P., Bellieni, G., Dudek, A., Efremova, S., Keller, J.,
858 Lameyre, J., Sabine, P.A., Schmid, R., Sørensen, H., Woolley, A.R., 2002. Igneous Rocks: A Classification and Glossary of Terms.
859 Recommendation of the International Union of Geological Sciences Subcommittee on the Systematics of Igneous Rocks, 2nd Edition.
860 Cambridge University Press, Cambridge. 236 pages.
- 861 Lee, J.Y., Marti, K., Severinghaus, J.P., Kawamura, K., Yoo, H.S., Lee, J.B., Kim, J.S., 2006. A redetermination of the isotopic abundances
862 of atmospheric Ar. *Geochim. Cosmochim. Acta* **70** (17), 4507-4512. <https://doi.org/10.1016/j.gca.2006.06.1563>.
- 863 Leicher, N., Giaccio, B., Zanchetta, G., Sulpizio, R., Albert, P.G., Tomlinson, E.L., Lagos, M., Francke, A., Wagner, B., 2021. Lake Ohrid's
864 tephrochronological dataset reveals 1.36 Ma of Mediterranean explosive volcanic activity. *Sci. Data* **8**, 231.
865 <https://doi.org/10.1038/s41597-021-01013-7>.
- 866 Leicher, N., Zanchetta, G., Sulpizio, R., Giaccio, B., Wagner, B., Nomade, S., Francke, A., Del Carlo, P., 2016. First tephrostratigraphic
867 results of the DEEP site record from Lake Ohrid (Macedonia and Albania). *Biogeosciences* **13**, 2151-2178. <https://doi.org/10.5194/bg-13-2151-2016>.
- 868
- 869 Lucchi, F., Keller, J., Tranne, C.A., 2013. Regional stratigraphic correlations across the Aeolian archipelago (southern Italy). In: Geological
870 Society, London, Memoirs, vol. 37, Chapter 6, pp. 55-81. <https://doi.org/10.1144/M37.6>.

- 871 Ludwig, K.R., 2001. Isoplot 3.0a geochronological toolkit for Microsoft Excel. In: Special Publication No. 4. Berkeley Geochronology
872 Center, Berkeley, CA, USA.
- 873 Marciano, R., Munno, R., Paola, P., Nicoletta, S., Santo, A., Villa, I., 2008. Late quaternary tephra layers along the Cilento coastline
874 (southern Italy). *J. Volcanol. Geotherm. Res.* **177** (1), 227-243. <https://doi.org/10.1016/j.jvolgeores.2007.11.009>.
- 875 Marianelli, P. & Sbrana, A. Risultati di misure standard di minerali e di vetri naturali in microanalisi a dispersione di energia (In Italian). *Atti*
876 *Soc. Tosc. Sci. Nat. Resid. Pisa, Mem. Serie A* **105**, 57-63 (1998).
- 877 Milner, A.M., Collier, R.E.L., Roucox, K.H., Müller, U.C., Pross, J., Kalaitzidis, S., Christanis, K., Tzedakis, P.C., 2012. Enhanced
878 seasonality of precipitation in the Mediterranean during the early part of the Last Interglacial. *Geology* **40** (10), 919-922.
879 <https://doi.org/10.1130/G33204.1>.
- 880 Milner, A.M., Müller, U.C., Roucox, K.H., Collier, R.E., Pross, J., Kalaitzidis, S., Christanis, K., Tzedakis, P.C., 2013. Environmental
881 variability during the Last Interglacial: a new high-resolution pollen record from Tenaghi Philippon, Greece. *J. Quat. Sci.* **28**, 113– 117.
882 <https://doi.org/10.1002/jqs.2617>.
- 883 Milner, A.M., Roucox, K.H., Collier, R.E. L., Müller, U.C., Pross, J., Tzedakis, P.C., 2016. Vegetation responses to abrupt climatic
884 changes during the Last Interglacial Complex (Marine Isotope Stage 5) at Tenaghi Philippon, NE Greece. *Quat. Sci.*
885 *Rev.* **154**, 169– 181. <https://doi.org/10.1016/j.quascirev.2016.10.016>.
- 886 Monaco, L., Palladino, D.M., Gaeta, M., Marra, F., Sottili, G., Leicher, N., Mannella, G., Nomade, S., Pereira, A., Regattieri, E., Wagner,
887 B., Zanchetta, G., Albert, P.G., Arienzo, I., D'Antonio, M., Petrosino, P., Manning, C., Giaccio, B., 2021. Mediterranean
888 tephrostratigraphy and peri-Tyrrhenian explosive activity reevaluated in light of the 430-365 ka record from Fucino Basin (central Italy).
889 *Earth Sci. Rev.* **220**, 103706. <https://doi.org/10.1016/j.earscirev.2021.103706>.
- 890 Morabito, S., Petrosino, P., Milia, A., Sprovieri, M., Tamburrino, S., 2014. A multidisciplinary approach for reconstructing the stratigraphic
891 framework of the last 40 ka in a bathyal area of the eastern Tyrrhenian Sea. *Glob. Planet Change* **123** (A), 121-138.
892 <https://doi.org/10.1016/j.gloplacha.2014.10.005>.
- 893 Munno, R. & Petrosino, P., 2007. The late Quaternary tephrostratigraphical record of the San Gregorio Magno basin (southern Italy). *J.*
894 *Quat. Sci.* **22**, 247-266. <https://doi.org/10.1002/jqs.1025>.
- 895 North Greenland Ice-Core Project members, Andersen, K.K., Azuma, N., Barnola, J.M., Bigler, M., Biscaye, P., Caillon, N., Chappellaz,
896 J., Clausen, H.B., Dahl-Jensen, D., Fischer, H., Flückiger, J., Fritzsche, D., Fujii, Y., Goto-Azuma, K., Grønbold, K., Gundestrup,
897 N.S., Hansson, M., Huber, C., Hvidberg, C.S., Johnsen, S.J., Jonsell, U., Jouzel, J., Kipfstuhl, S., Landais, A., Leuenberger,
898 M., Lorrain, R., Masson-Delmotte, V., Miller, H., Motoyama, H., Narita, H., Popp, T., Rasmussen, S.O., Raynaud, D., Röthlisberger,
899 R., Ruth, U., Samyn, D., Schwander, J., Shoji, H., Siggard-Andersen, M.L., Steffensen, J.P., Stocker, T., Sveinbjörnsdóttir,
900 A.E., Svensson, A., Takata, M., Tison, J. L., Thorsteinsson, T., Watanabe, O., Wilhelms, F., White, J., 2004. High-resolution record of
901 the Northern Hemisphere climate extending into the last interglacial period. *Nature* **431**, 147-151.
- 902 Niespolo, E.M., Rutte, D., Deino, A.L., Renne, P.R., 2017. Intercalibration and age of the Alder Creek Sanidine ⁴⁰Ar/³⁹Ar standard. *Quat.*
903 *Geochronol.* **39**, 205-213. <https://doi.org/10.1016/j.quageo.2016.09.004>.
- 904 Pabst, S., Wörner, G., Civetta, L., Tesoro, R., 2007. Magma chamber evolution prior to the Campanian Ignimbrite and Neapolitan Yellow
905 Tuff eruptions (Campi Flegrei, Italy). *Bull. Volcanol.* **70**, 961-976. <https://doi.org/10.1007/s00445-007-0180-z>.
- 906 Pappalardo, L., Civetta, L., D'Antonio, M., Deino, A., Di Vito, M., Orsi, G., Carandente, A., de Vita, S., Isaia, R., Piochi, M., 1999. Chemical
907 and Sr-isotopical evolution of the Phlegrean magmatic system before the Campanian Ignimbrite and the Neapolitan Yellow Tuff
908 eruptions. *J. Volcanol. Geotherm. Res.* **91** (2-4), 141-166. [https://doi.org/10.1016/S0377-0273\(99\)00033-5](https://doi.org/10.1016/S0377-0273(99)00033-5).
- 909 Paterne, M., Guichard, F., Duplessy, J.C., Siani, G., Sulpizio, R., Labeyrie, J., 2008. A 90,000-200,000 yrs marine tephra record of Italian
910 volcanic activity in the Central Mediterranean Sea. *J. Volcanol. Geotherm. Res.* **177**, 187-196.
911 <https://doi.org/10.1016/j.jvolgeores.2007.11.028>.
- 912 Paterne, M., Guichard, F., Labeyrie, J., 1988. Explosive activity of the south Italian volcanoes during the past 80,000 years as determined
913 by marine tephrochronology. *J. Volcanol. Geotherm. Res.* **34**, 153-172. [https://doi.org/10.1016/0377-0273\(88\)90030-3](https://doi.org/10.1016/0377-0273(88)90030-3).
- 914 Paterne, M., Guichard, F., Labeyrie, J., Gillot, P.Y., Duplessy, J.C., 1986. Tyrrhenian Sea tephrochronology of the oxygen isotope record
915 for the past 60,000 years. *Mar. Geol.* **72**, 259-285. [https://doi.org/10.1016/0025-3227\(86\)90123-4](https://doi.org/10.1016/0025-3227(86)90123-4).
- 916 Pelullo, C., Cirillo, G., Iovine, R.S., Arienzo, I., Aulinas, M., Pappalardo, L., Petrosino P., Fernandez-Turiel, J.L., D'Antonio, M., 2020.
917 Geochemical and Sr-Nd isotopic features of the Zaro volcanic complex: insights on the magmatic processes triggering a small-scale
918 prehistoric eruption at Ischia island (south Italy). *Int. J. Earth Sci.* **109** (8), 2829-2849. <https://doi.org/10.1007/s00531-020-01933-6>.
- 919 Peccerillo, A., 2017. Cenozoic Volcanism in the Tyrrhenian Sea Region. In: IAVCEI, Advances in Volcanology, 2 ed. Springer, p. 400.
- 920 Petrosino, P., Arienzo, I., Mazzeo, F.C., Natale, J., Petrelli, M., Milia, A., Perugini, D., D'Antonio, M., 2019. The San Gregorio Magno
921 lacustrine basin (Campania, southern Italy): improved characterization of the tephrostratigraphic markers based on trace elements
922 and isotopic data. *J. Quat. Sci.* **34**, 393-404. <https://doi.org/10.1002/jqs.3107>.
- 923 Petrosino, P., Jicha, B.R., Mazzeo, F.C., Ciaranfi, N., Girone, A., Maiorano, P., 2015. The Montalbano Jonico marine succession: An
924 archive for distal tephra layers at the Early-Middle Pleistocene boundary in southern Italy. *Quat. Int.* **383**, 89-103.
925 <https://doi.org/10.1016/j.quaint.2014.10.049>.
- 926 Petrosino, P., Morabito, S., Jicha, B.R., Milia, A., Sprovieri, M., Tamburrino, S., 2016. Multidisciplinary tephrochronological correlation of
927 marker events in the eastern Tyrrhenian Sea between 48 and 105 ka. *J. Volcanol. Geotherm. Res.* **315**, 79-99.
928 <https://doi.org/10.1016/j.jvolgeores.2016.02.001>.
- 929 Poli, S., Chiesa, S., Gillot, P.-Y., Gregnanin, A., Guichard, F., 1987. Chemistry versus time in the volcanic complex of Ischia (Gulf of
930 Naples, Italy): evidence of successive magmatic cycles. *Contrib. Mineral. Petrol.* **95**, 322-335.
- 931 Rasmussen, S.O., Bigler, M., Blockley, S.P., Blunier, T., Buchardt, S.L., Clause, H.B., Cvijanovic, I., Dahl-Jensen, D., Johnsen, S.J.,
932 Fischer, H., Gkinis, V., Guillevic, M., Hoek, W.Z., Lowe, J.J., Pedro, J.B., Popp, T., Seierstad, I.K., Steffensen, J.P., Svensson, A.M.,
933 Vallelonga, P., Vinther, P.M., Walker, M.J.C., Wheatley, J.J., Winstrup, M., 2014. A stratigraphic framework for abrupt climatic changes
934 during the Last Glacial period based on three synchronized Greenland ice-core records: refining and extending the INITIMATE event
935 stratigraphy. *Quat. Sci. Rev.* **106**, 14-28. <https://doi.org/10.1016/j.quascirev.2014.09.007>.

- 936 Regattieri, E., Giaccio, B., Nomade, S., Francke, A., Vogel, H., Drysdale, R.N., Perchiazzi, N., Wagner, B., Gemelli, M., Mazzini, I., Boschi,
937 C., Galli, P., Peronace, E., 2017. A Last Interglacial record of environmental changes from the Sulmona Basin (central Italy).
938 *Palaeogeogr. Palaeoclimatol. Palaeoecol.* **472**, 51-66. <https://doi.org/10.1016/j.palaeo.2017.02.013>.
- 939 Regattieri, E., Giaccio, B., Zanchetta, G., Drysdale, R.N., Galli, P., Nomade, S., Peronace, E., Wulf, S., 2015. Hydrological variability over
940 the Apennines during the Early Last Glacial precession minimum, as revealed by a stable isotope record from Sulmona basin, Central
941 Italy. *J. Quat. Sci.* **30**, 19-31. <https://doi.org/10.1002/jqs.2755>.
- 942 Renne, P.R., Balco, G., Ludwig, K.R., Mundil, R., Min, K., 2011. Response to the comment by WH Schwarz et al. on "Joint determination
943 of 40 K decay constants and ⁴⁰Ar*/⁴⁰K for the Fish Canyon sanidine standard, and improved accuracy for ⁴⁰Ar/³⁹Ar geochronology" by
944 PR Renne et al. (2010). *Geochim. Cosmochim. Acta* **75**, 5097-5100.
- 945 Rolandi, G., Bellucci, F., Heizler, M.T., Belkin, H.E., De Vivo, B., 2003. Tectonic controls on the genesis of ignimbrite from the Campanian
946 Volcanic Zone, southern Italy. *Mineral. Petrol.* **79**, 3-31. <https://doi.org/10.1007/s00710-003-0014-4>.
- 947 Rosi, M., Sbrana, A., Vezzoli, L., 1988a. Tephrostratigraphy of Ischia, Procida and Campi Flegrei volcanic products (In Italian). *Mem. Soc.*
948 *Geol. It.* **41**, 1015-1027.
- 949 Rosi, M., Sbrana, A., Vezzoli, L., 1988b. Stratigraphy of Procida and Vivara islands (In Italian). *Boll. GNV* **4**, 500-525.
- 950 Santacroce, R. & Sbrana, A., 2003. Geological map of Vesuvius, 1:15.000 scale. SELCA, Firenze.
- 951 Santacroce, R., Cioni, R., Marianelli, P., Sbrana, A., Sulpizio, R., Zanchetta, G., Donahue, D.J., Joron, J.L., 2008. Age and whole rock-
952 glass compositions of proximal pyroclastics from the major explosive eruptions of Somma-Vesuvius: A review as a tool for distal
953 tephrostratigraphy. *J. Volcanol. Geotherm. Res.* **177**, 1-18. <https://doi.org/10.1016/j.jvolgeores.2008.06.009>.
- 954 Satow, C., Tomlinson, E.L., Grant, K.M., Albert, P.G., Smith, V.C., Manning, C.J., Ottolini, L., Wulf, S., Rohling, E.J., Lowe, J.J., Blockley,
955 S.P.E., Menzies, M.A., 2015. A new contribution to the Late Quaternary tephrostratigraphy of the Mediterranean: Aegean Sea core
956 LC21. *Quat. Sci. Rev.* **117**, 96-112. <https://doi.org/10.1016/j.quascirev.2015.04.005>.
- 957 Scarpati, C., Perrotta, A., Lepore, S., Calvert, A., 2013. Eruptive history of the Neapolitan volcanoes: constraints from ⁴⁰Ar-³⁹Ar dating.
958 *Geol. Mag.* **150** (3), 412-425. <https://doi.org/10.1017/S0016756812000854>.
- 959 Shackleton, N.J., Fairbanks, R.G., Chiu, T., Parenin, F., 2004. Absolute calibration of the Greenland time scale: implications for the
960 Antarctic time scales and for $\Delta^{14}\text{C}$. *Quat. Sci. Rev.* **23** (14-15), 1513-1522. <https://doi.org/10.1016/j.quascirev.2004.03.006>.
- 961 Sinopoli, G., Masi, A., Regattieri, E., Wagner, B., Francke, A., Peyron, O., Sadori, L., 2018. Palynology of the Last Interglacial Complex
962 at Lake Ohrid: palaeoenvironmental and palaeoclimatic inferences. *Quat. Sci. Rev.* **180**, 177-192.
963 <https://doi.org/10.1016/j.quascirev.2017.11.013>.
- 964 Smith, V.C., Isaia, R., Engwell, S.L., Albert, P.G., 2016. Tephra dispersal during the Campanian Ignimbrite (Italy) eruption: implications
965 for ultra-distal ash transport during the large caldera-forming eruption. *Bull. Volcanol.* **78**, 45. <https://doi.org/10.1007/s00445-016-1037-0>.
- 966 Smith, V.C., Isaia, R., Pearce, N.J.G., 2011. Tephrostratigraphy and glass compositions of post-15 kyr Campi Flegrei eruptions: implications
967 for eruption history and chronostratigraphic markers. *Quat. Sci. Rev.* **30**, 3638-3660.
- 968 Sulpizio, R., Zanchetta, G., D'Orazio, M., Vogel, H., Wagner, B., 2010. Tephrostratigraphy and tephrochronology of lakes Ohrid and
969 Prespa, Balkans. *Biogeosciences* **7**, 3273-3288. <https://doi.org/10.5194/bg-7-3273-2010>.
- 970 Tomlinson, E.L., Albert, P.G., Wulf, S., Brown, R.J., Smith, V.C., Keller, J., Orsi, G., Bourne, A., Menzies, M.A., 2014. Age and
971 geochemistry of tephra layers from Ischia, Italy: constraints from proximal-distal correlations with Lago Grande di Monticchio. *J.*
972 *Volcanol. Geotherm. Res.* **287**, 22-39. <https://doi.org/10.1016/j.jvolgeores.2014.09.006>.
- 973 Tomlinson, E.L., Arienzo, I., Civetta, L., Wulf, S., Smith, V.C., Hardiman, M., Lane, C.S., Carandente, A., Orsi, G., Rosi, M., Müller, W.,
974 Menzies, M.A., 2012. Geochemistry of the Phlegrean Fields (Italy) proximal sources for major Mediterranean tephras: Implications for
975 the dispersal of Plinian and co-ignimbritic components of explosive eruptions. *Geochim. Cosmochim. Acta* **93**, 102-128.
976 <https://doi.org/10.1016/j.gca.2012.05.043>.
- 977 Tomlinson, E.L., Thordarson, T., Muller, W., Thirlwall, M.T., Menzies, M.A., 2010. Microanalysis of tephra by LA-ICP-MS - strategies,
978 advantages and limitations assessed using the Thorsmork ignimbrite (Southern Iceland). *Chem. Geol.* **279**, 73-89.
979 <https://doi.org/10.1016/j.chemgeo.2010.09.013>.
- 980 Tonarini, S., D'Antonio, M., Di Vito, M.A., Orsi, G., Carandente, A., 2009. Geochemical and Ba-Sr-Nd isotopic evidence for mingling and
981 mixing processes in the magmatic system that fed the Astroni volcano (4.1-3.8 ka) within the Campi Flegrei caldera (southern Italy).
982 *Lithos* **107** (3-4), 135-151. <https://doi.org/10.1016/j.lithos.2008.09.012>.
- 983 Wagner, B., Wilke, T., Francke, A., Albrecht, C., Baumgarten, H., Bertini, A., Combourieu-Nebout, N., Cvetkoska, A., D'Addabbo, M.,
984 Donders, T.H., Föller, K., Giaccio, B., Grazhdani, A., Hauffe, T., Holtvoeth, J., Joannin, S., Jovanovska, E., Lust, J., Kouli, K.,
985 Koutsodendris, A., Krastel, S., Lacey, J.H., Leicher, N., Leng, M.J., Levkov, Z., Lindhorst, K., Masi, A., Mercuri, A.M., Nomade, S.,
986 Nowaczyk, N., Panagiotopoulos, K., Peyron, O., Reed, J.M., Regattieri, E., Sadori, L., Sagnotti, L., Stelbrink, B., Sulpizio, R.,
987 Tofilovska, S., Torri, P., Vogel, H., Wagner, T., Wagner-Cremer, F., Wolff, G.A., Wonik, T., Zanchetta, G., Zhang, X.S., 2017. The
988 environmental and evolutionary history of Lake Ohrid (FYROM/Albania): interim results from the SCOPSCO deep drilling project.
989 *Biogeosciences* **14**, 2033-2054. <https://doi.org/10.5194/bg-14-2033-2017>.
- 990 Wagner, B., Vogel, H., Francke, A., Friederich, T., Donders, T., Lacey, J.H., Leng, M.J., Regattieri, E., Sadori, L., Wilke, T., Zanchetta,
991 G., Albrecht, C., Bertini, A., Combourieu-Nebout, N., Cvetkoska, A., Giaccio, B., Grazhdani, A., Hauffe, T., Holtvoeth, J., Joannin, S.,
992 Lagoos, M., Leicher, N., Levkov, Z., Lindhorst, K., Masi, A., Melles, M., Mercuri, A.M., Nomade, S., Nowaczyk, N., Panagiotopoulos,
993 K., Peyron, O., reed, J.M., Sagnotti, L., Sinopoli, G., Stellbrink, B., Sulpizio, R., Timmermann, A., Tofilovska, S., Torri, P., Wagner-
994 Cremer, F., Wonik, T., Zhang, X., 2019. Mediterranean winter rainfall in phase with African monsoons during the past 1.36 million
995 years. *Nature* **573**, 256-260. <https://doi.org/10.1038/s41586-019-1529-0>.
- 996 Wulf, S., Hardiman, M.J., Staff, R.A., Koutsodendris, A., Appelt, O., Blockley, S.P.E., Lowe, J.J., Manning, C.J., Ottolini, L., Schmitt, A.K.,
997 Smith, V.C., Tomlinson, E.L., Vakhrameeva, P., Knipping, M., Kotthoff, U., Milner, A.M., Müller, U.C., Christianis, K., Kalaitzidis, S.,
998 Tzedakis, P.C., Schmiiedl, G., Pross, J., 2018. The Marine isotope stage 1-5 cryptotephra record of Tenaghi Philippon, Greece:
999 Towards a detailed tephrostratigraphic framework for the Eastern Mediterranean region. *Quat. Sci. Rev.* **186**, 236-262.
1000 <https://doi.org/10.1016/j.quascirev.2018.03.011>.
- 1001

1002 Wulf, S., Keller, J., Paterne, M., Mingram, J., Lauterbach, S., Opitz, S., Sottili, G., Giaccio, B., Albert, P.G., Satow, C., Tomlinson, E.L.,
1003 Viccaro, M., Brauer, A., 2012. The 100-133 ka record of Italian explosive volcanism and revised tephrochronology of Lago Grande di
1004 Monticchio. *Quat. Sci. Rev.* **58**, 104-123. <https://doi.org/10.1016/j.quascirev.2012.10.020>.
1005 Wulf, S., Kraml, M., Brauer, A., Keller, J., Negendank, J.F.W., 2004. Tephrochronology of the 100 ka lacustrine sediment record of Lago
1006 Grande di Monticchio (Southern Italy). *Quat. Int.* **122**, 7-30. <https://doi.org/10.1016/j.quaint.2004.01.028>.
1007 Wulf, S., Kraml, M., Keller, J., 2008. Towards a detailed tephrostratigraphy in the Central Mediterranean: The last 20,000 yrs record of
1008 Lago Grande di Monticchio. *J. Volcanol. Geotherm. Res.* **177**, 118-132. <https://doi.org/10.1016/j.jvolgeores.2007.10.009>.
1009 Zanchetta, G., Giaccio, B., Bini, M., Sarti, L., 2018. Tephrostratigraphy of Grotta del Cavallo, Southern Italy: insights of the chronology of
1010 Middle to Upper Paleolithic transition in the Mediterranean. *Quat. Sci. Rev.* **182**, 65-77.
1011 <https://doi.org/10.1016/j.quascirev.2017.12.014>.
1012 Ziegler, M., Tuenter, E., Lourens, L.J. 2010. The precession phase of the boreal summer monsoon as viewed from the eastern
1013 Mediterranean (ODP Site 968). *Quat. Sci. Rev.* **29** (11-12), 1481-1490. <https://doi.org/10.1016/j.quascirev.2010.03.011>.
1014